PSFC/JA-07-01

Plasma-surface interaction, scrape-off layer and divertor physics: Implications for ITER

B. Lipschultz[1], X. Bonnin[2], G. Counsell[3], A. Kallenbach[4], A. Kukushkin[5], K. Krieger[4], A. Leonard[6], A. Loarte[7], R. Neu[4], R.A. Pitts[8], T. Rognlien[9], J. Roth[4], C. Skinner[10], J.L. Terry[1], E. Tsitrone[11], D. Whyte[1], S. Zweben[10], N. Asakura[12], D. Coster[4], R. Doerner[13], R. Dux[4], G. Federici[7], M. Fenstermacher[9], W. Fundamenski[3], P. Ghendrih[11], A. Herrmann[4], J. Hu[14], S. Krasheninnikov[13], G. Kirnev[15], A. Kreter[16], V. Kurnaev[17], B. LaBombard[1], S. Lisgo[18], T. Nakano[12], N. Ohno[19], H.D. Pacher[20], J. Paley[3], Y. Pan[21], G. Pautasso[4], V. Philipps[16], V. Rohde[4], D. Rudakov[13], P. Stangeby[18], S. Takamura[19], T. Tanabe[22], Y. Yang[14], S. Zhu[14]

July 2007

Plasma Science and Fusion Center
Massachusetts Institute of Technology
Cambridge MA 02139 USA

[1]MIT - Cambridge, MA, USA
[2]U. Paris – Paris, France
[3]UKAEA – Culham, UK
[4]MPI-IPP - Garching, Germany
[5]ITER Team - Garching, Germany
[6]DIII-D - San Diego, CA, USA
[7]EFDA- Garching, Germany
[8]CRPP-EPFL - Lausanne, Switzerland
[9]LLNL - Livermore, CA, USA
[10]PPPL - Princeton, NJ, USA
[11]CEA - Cadarache, France
[12]JAEA – Naka, Japan
[13]CER - La Jolla, CA, USA
[14]ASIPP - Hefei, China
[15]Kurchatov Institute - Moscow, Russia
[16]FZ - Jülich, Germany
[17]MEPI - Moscow, Russia
[18]UTIAS – Toronto, Canada
[19]Nagoya U. - Nagoya, Japan
[20]INRS-EMT – Québec, Canada
[21]SWIPP - Chengdu, China
[22]Kyushu U. - Kyushu, Japan

This work was supported by the U.S. Department of Energy, Grant No. DE-FC02-99ER54512.

Submitted for publication to *Nuclear Fusion*.

Plasma-surface interaction, scrape-off layer and divertor physics: Implications for ITER

B Lipschultz[1], X Bonnin[2], G Counsell[3], A Kallenbach[4], A Kukushkin[5], K Krieger[4], A Leonard[6], A Loarte[7], R Neu[4], R A Pitts[8], T. Rognlien[9], J Roth[4], C Skinner[10], J L Terry[1], E Tsitrone[11], D Whyte[1], S Zweben[10], N Asakura[12], D Coster[4], R Doerner[13], R Dux[4], G Federici[7], M Fenstermacher[9], W Fundamenski[3], P Ghendrih[11], A Herrmann[4], J Hu[14], S Krasheninnikov[13], G Kirnev[15], A Kreter[16], V Kurnaev[17], B LaBombard[1], S Lisgo[18], T Nakano[12], N Ohno[19], H D Pacher[20], J Paley[3], Y Pan[21], G Pautasso[4], V Philipps[16], V Rohde[4], D Rudakov[13], P Stangeby[18], S Takamura[19], T Tanabe[22], Y Yang[14], S Zhu[14]

[1]Massachusetts Institute of Technology, Plasma Science and Fusion Center, 175 Albany Street, Cambridge, MA 02319, USA

[2]LIMHP, CNRS-UPR 1311, Université Paris 13, 99 Avenue J.-B. Clément F-93430 Villetaneuse, FRANCE

[3]Association Euratom-UKAEA Fusion Association, Culham Science Research Centre, Abingdon OX113, UK

[4]Association Euratom-Max Planck Insitut fur Plasmaphysik, D-85748, Germany

[5]ITER International Team, Garching Working Site, D-85748, Germany

[6]DIII-D National Fusion Facility, P.O. Box 85608, San Diego CA 92186, USA

[7]EFDA, Close Support Unit Garching, D-85748 Garching, Germany

[8]CRPP-EPFL, Association EURATOM-Confederation Suisse, 1015 Lausanne, Switzerland

[9]Lawrence Livermore National Laboratory, P.O. Box 808 / L-637 Livermore, CA 94551

[10]Princeton Plasma Physics Laboratory, P. O. Box 451, Princeton, NJ 08543

[11]Association Euratom-CEA, CEA/DSM/DRFC, CEA Cadarache, F-12108 St. Paul-lez-Durance, France

[12]Japan Atomic Energy Agency, Naka site, Naka, Ibaraki 311-0193, Japan

[13]Center for Energy Research, 9500 Gilman Dr., UCSD, La Jolla, CA. 92093-0417, USA

[14]Academy Sinica Institute of Plasma Physics, Hefei, China

[15]Nuclear Fusion Institute, RRC "Kurchatov Institute", Kurchatov sq. 1, 123182, Moscow, Russia

[16]Association Euratom-Forschungszentrum Jülich, GMBH, D-52425, Jülich Germany

[17]Moscow Engineering Physics Institute 141980 Dubna, Moscow Region, Russia

[18]University of Toronto Institute for Aerospace Studies, 4925 Dufferin St., Toronto, M3H 5T6, Canada

[19]Department of Energy Engineeing and Science, Graduate School of Engineering, Nagoya University Nagoya 464-8603, Japan

[20]INRS-EMT, 1650 boul. Lionel Boulet, Varennes, Québec J3X 1S2, CANADa

[21]Southwestern Institute of Plasma Physics, Chengdu, China

[22]Department of Advanced Energy Engineering Science, Kyushu University 6-10-1, Hakozaki, Higashi-ku, Fukuoka 812-8581, Japan

E-mail contact: blip@psfc.mit.edu

Abstract: Recent research in Scrape-Off Layer (SOL) and divertor physics is reviewed; New and existing data from a variety of experiments have been used to make cross-experiment comparisons with implications for further research and ITER. Studies of the region near the separatrix have addressed the relationship of profiles to turbulence as well as the scaling of the parallel power flow. Enhanced low-field side radial transport is implicated as driving parallel flows to the inboard side. The medium-n nature of Edge Localized Modes (ELMs) has been elucidated and new measurements have determined that they carry ~10-20% of the ELM energy to the far SOL with implications for ITER limiters and the upper divertor. The predicted divertor power loads for ITER disruptions are reduced while those to main chamber PFCs increase. Disruption mitigation through massive gas puffing is successful at reducing PFC heat loads. New estimates of ITER tritium retention have shown tile sides to play a significant role; Tritium cleanup may be necessary every few days to weeks. ITER's use of mixed materials gives rise to a reduction of surface melting temperatures and chemical sputtering. Advances in modelling of the ITER divertor and flows have enhanced the capability to match experimental data and predict ITER performance.

PACS: 52.25.Fi, 52.35.Ra, 52.40.Hf, 52.55.Fa, 52.55.Rk

Submitted to Nuclear Fusion

1. Introduction

The interaction of plasma with surrounding Plasma Facing Component (PFC) surfaces will have considerable impact on the performance of fusion plasmas, the lifetime of PFCs, and the retention of tritium in next step Burning Plasma Experiments, such as ITER. This paper on recent Scrape-Off Layer (SOL) & divertor physics research, primarily the work of the International Tokamak Physics Activity (ITPA) SOL/Divertor group, reviews the considerable progress achieved in the last several years. Earlier, more in-depth reviews of work in this area, are available [1-3].

2. Transport

Recent research has provided insight on the physics that controls the steady-state transport and cross-field profiles that are observed in the Scrape-Off-Layer (SOL). Studies of the density and temperature profiles just outside the separatrix (within one density scale length, λ_n – the 'near' SOL) in C-Mod [4] have shown that the local radial pressure gradient, ∇p,

depends on the local normalized collisionality, ν^* (ν_{ee}/L, where ν_{ee} is the electron-electron collisionality and L is the connection length from the midplane to the divertor). Moreover, a potential connection to the underlying turbulence that determines the gradients is made: at fixed values of normalized collisionality parameter (characterized as the 'diamagnetic parameter', α_d), electron pressure gradients in the near SOL increase with plasma current squared, holding the MHD ballooning parameter, α_{MHD} [5, 6], constant. A parallel analysis of ASDEX-Upgrade density and temperature scale lengths in the region of the separatrix (both inside and outside) during ELMy H-modes [7] showed that the temperature decay length, λ_T, correlates with the density decay length, λ_n, as $\eta_e = \lambda_n/\lambda_T \approx 2$. Reference [7] indicates that an inward particle pinch, driven by drift-wave turbulence, should drive η_e to a limiting value of 2.

While the above single-machine analyses potentially give new insight into the connection of steady-state profiles to the underlying physics of radial transport, empirical extrapolation can also be made to ITER. A multi-machine database of plasma profiles in the region of the separatrix has been compiled and analyzed for the local temperature gradients under the assumption that electron thermal conductivity is dominant (ion channel ignored) [8]. Thomson profile data was utilized for all tokamaks in the database. The Thomson data was augmented by data from Li beam (JET) and Langmuir probes (JT-60U). All data were time-averaged over H-mode ELMs. The was a range in input power for each tokamak (ASDEX-Upgrade: 2.5 - 7.5MW, DIII-D: 1.4 - 6.2MW, JET: 6.9 – 16.5, C-Mod: 1.6 – 4.0MW, JT-60U: 4.5 – 5.5MW). Based on that database and the known relationship between SOL parallel power flow (conduction) and temperature e-folding lengths mapped to the low-field side midplane, namely $\lambda_q = 2\lambda_T/7$ [9], one can derive λ_q for those tokamaks included in the study. The result is shown in Fig. 1 where the power flow gradient scale length normalized to device linear size (R, major radius), λ_q/R, is seen to be approximately constant within the significant scatter of the data. Such a scaling indicates that the resultant peak parallel power flow in the SOL, $q_{\parallel,0}$, which is proportional to $P_{SOL}Aq_{95}/(R\lambda_q)$, scales as

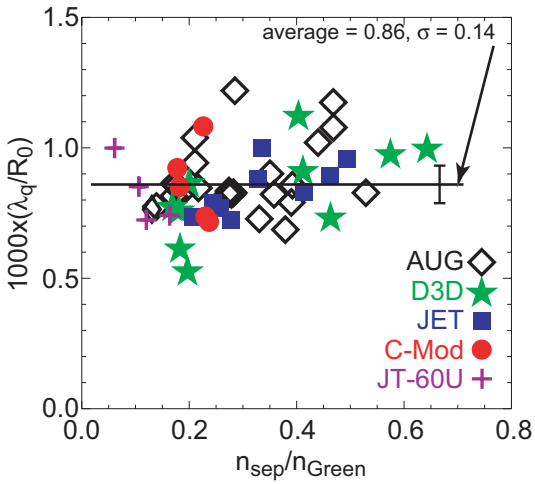

Figure 1: Ratio of parallel power e-folding length, λ_q, to device major radius, plotted vs separatrix density normalized to the Greenwald density. The average and standard deviation for the dataset are shown.

P_{SOL}/R^2 if one holds the aspect ratio, A, and edge safety factor, $q_{95,}$, and therefore normalized connection length, constant. There are several implications of such a scaling: First, it surprisingly suggests that present devices in fact span the level of parallel power flow density (W/m^2) predicted for ITER (see Table 1), allowing direct empirical comparisons

Parameter	C-Mod	DIII-D	JET	ITER
a (m)	.22	.6	1.2	2
R (m)	0.67	1.7	2.96	6.2
$P_{AUX,max}$ (MW)	6.0	15	25	50
Pα (MW)	0	0	0	80
P/R (MW/m)	9	8.8	8.5	21
P/R^2 (MW/m^2)	13.4	5.2	2.9	3.4

Table 1: Comparison of the operating parameters (maximum auxiliary heating power) for various tokamaks with that of ITER. ASDEX-Upgrade and JT-60U are assume to be essentially the same as DIII-D and JET respectively for this comparison.

between present devices and ITER. Second, it appears that λ_q proportional to R is at odds with the popular use of the SOL P/R scaling [10], which fundamentally sets the requirements for matching SOL temperature scale lengths across devices through dimensionless arguments, as also being the important figure of merit for heat exhaust (e.g. [11]). The linear scaling with major radius of Fig. 1 extrapolates to a λ_q for ITER of order 6 mm with significant uncertainty. We have more confidence in the λ_q dependence on R than in the absolute value predicted for ITER at this time. On the other hand the prediction of this multi-machine study is similar to other extrapolations of midplane λ_q to ITER based on analysis of ELM-averaged divertor power deposition profiles [12, 13]. Lastly, such short values of λ_q are also predicted by modeling of ITER [14]. It is important to note that the modeled parallel power flow profile incident on the divertor is not as narrow as that predicted from the above empirical scalings; Flux expansion in the divertor region lowers the parallel flow per unit area of flux tube. Experimentally, it is found that there can be an additional factor of three or more broadening of the heat load profile at the divertor plate beyond that due merely to flux expansion, probably the result of higher power losses (primarily radiation) near the separatrix relative to farther out in the SOL. It is also possible that the observed divertor heat load broadening may be due to enhanced cross-field heat transport there and/or the effect of flux tubes passing close to the x-point. Further studies are needed to confirm the scaling indicated in Fig. 1 in absolute value as well as with regard to potential dependencies on power. In addition we must compare the divertor heat load

profiles with that obtained upstream to better understand the processes that are playing a role in heat load broadening.

Further from the separatrix (in the 'far' SOL) the density gradients are weaker leading to substantial densities there [15-17]. The inferred steady-state cross-field ion transport in the far SOL is convective during L-mode [18, 19] as well as during, and between, ELMs [19]. The inferred 'effective' convective radial velocity increases as a function of distance from the separatrix from $v_r \sim 20$ m/s to $\sim$ 100-200m/s. Dimensionless comparisons of this convective steady-state transport among three tokamaks (L-modes) shows little or no dependence on local dimensionless parameters (ρ^*, ν^*, β) [20, 18]. This characteristic independence of local parameters in the far SOL may be due to the blob filament being born at a point in the near SOL, far away, and thus not having local characteristics.

Based on the above convective velocities we can make an estimate of the radial ion fluxes in the ITER far SOL. Taking predicted density profiles for the ITER SOL [21], we select the density at the second separatrix radius (4 cm at the midplane) which corresponds to the edge of the model grid, $4x10^{18}$ m^{-3}. Given that the near SOL width scales roughly with major radius (4 mm in C-Mod [18], 1 cm in DIII-D [18], 2 cm in JET [20]) then the ITER second separatrix will be located near the transition between near and far SOL regions. The ITER radial convective velocity there would then be ~20m/s (v_r is independent of local plasma characteristics). Together with the ITER surface area, 940 m^2, the resultant total wall flux would then be ~$7.5x10^{22}$/s, a value similar to current tokamaks [22, 23]. This is probably a lower estimate of the wall fluxes and resultant Be source given that we do not yet know how flat the far SOL density profile will be nor can we predict the Be source due to ELMs (those issues will both be discussed later). Assuming a sputtering coefficient of 1%, the Be source would then be ~ $7.5x10^{20}$/s, again similar to the total C source rate in current tokamaks [24, 23, 3]. We can estimate the core B content by assuming reasonable values for impurity confinement time, τ_{imp}, at the level of the energy confinement time of 3.7s in ITER [1], a plasma volume, V_{ITER}, of ~ $840m^3$, and a high transmission of impurities through the SOL, η, of 0.1 (e.g. [25]). The core Be density is then given by $n_{Be} \sim \Gamma_{Be,influx} x\ \eta\ x(\tau_{imp}/V_{ITER}) \sim 3.5x10^{17}m^{-3}$. For ITER volume-averaged densities of order $1x10^{20}m^{-3}$ the impurity concentration would be of order 0.4% (Z_{eff} due to Be ~ .05).

Taking this prediction one step further we can examine what the Be erosion rate implies for T co-deposition with Be. On present devices such "main-wall" impurity source rates appear to set impurity film growth, and hence T co-deposition rates, at the inner divertor [23]. For a T co-deposition rate of ~0.1 T/B at surface temperatures ~ 200 ºC ([26] and other studies referenced therein) ITER PFCs would retain 7.5×10^{19}T/s or 0.15g T per 400s discharge, quite low. The uncertainty of the T co-deposition is very large given that the measured T/Be level has been measured to be very temperature dependent, dropping rapidly from of order 20% at room temperature to 1% at 400ºC. T retention in ITER is predicted to be higher than this simple estimate based on methods covered elsewhere in this paper such as post-campaign tile analysis and detailed transport modelling.

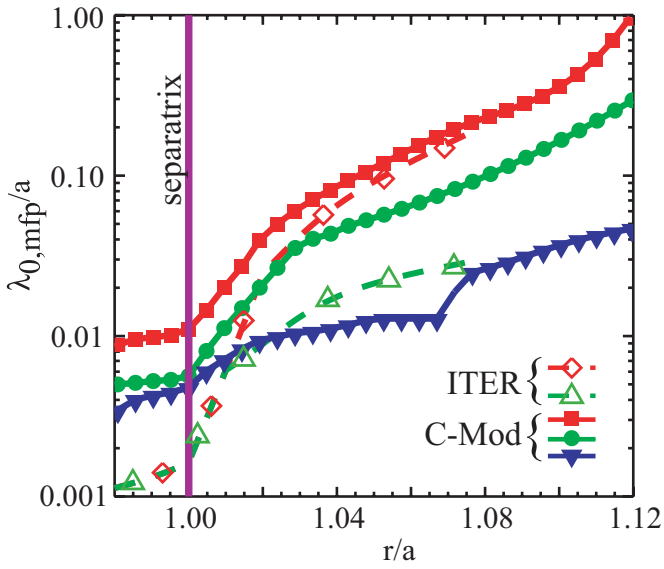

Figure 2: The mean free path for neutrals (due to ionization and charge exchange) vs normalized radius is shown for ITER and Alcator C-Mod. The ITER density profile for the 2 cases shown is the same from the separatrix to the edge of the model calculation. From that point further outward into the SOL we have assumed that the density either falls exponentially (lower opacity) or is flat (higher opacity). Three density cases for C-Mod are shown corresponding to $n/n_{Greenwald}$ of ~ 0.15, 0.22, and 0.36 [18]. The opacity increases as the density increases.

The above-referenced code prediction of the ITER SOL density profile [21] is based on diffusive transport in the SOL, not the convective transport described earlier. If, as speculated [20], the opacity of the SOL to recycled neutrals plays an important role in raising the density in the far SOL, then the ITER SOL density profile could be broader than presently predicted by fluid models. Again utilizing the model predictions of the ITER SOL density profile we can calculate the penetration of neutrals through it. In Figure 2 we have compared that calculation to that for the Alcator C-Mod SOL, which, of current tokamaks, most closely approaches the ITER conditions for neutral opacity. The C-Mod SOL density profiles can be very flat at densities far below the empirical Greenwald density limit [27] which ITER operates near to. The similarities to C-Mod raise the possibility that the ITER SOL will be broader than presently modeled based on pure diffusive transport leading to higher densities and higher radial fluxes than calculated above. Further understanding of

how radial ion fluxes scale to ITER, both for L- and H-mode, and the role of SOL opacity to neutrals, are needed to predict the steady state plasma wall interaction in ITER.

The emerging picture of how turbulent transport leads to the observed steady-state profiles is that instabilities in the near SOL give rise to plasma filaments (aligned along **B**), or 'blobs', that are radially ejected and carry plasma into the far SOL (100-500 m/s) [3]. Such behavior would be consistent with the convective characteristics derived from analysis of time-averaged profiles as discussed above. The streaming of such density clumps into the far SOL is also consistent with the tendency in many cases for the SOL profile to be flatter in that region in comparison to the near SOL; Under conditions where the neutral density in the far SOL is sufficient (opacity of the filaments to neutrals) the plasma in the filaments can be sustained by ionization, which competes against particle losses along open field lines [28].

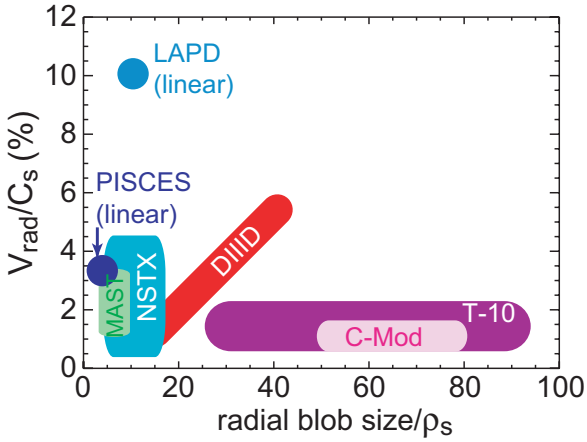

Figure 3: Turbulence filament cross-section size and radial velocity in the SOL normalized to the local ion Larmor radius at the electron temperature, ρ_s, and the local ion sound speed, c_s, for a number of devices.

We have abstracted the physical size and velocity of the blob filaments from published data for both tokamaks and linear devices [29-32, 15, 33-36] and normalized them to the local ρ_s and c_s respectively, Fig. 3. The appearance of radially moving filaments in a linear machine [33] has been attributed to interchange modes driven by the frictional force due to neutral flows. Note that two different primary techniques were used to obtain the measurements included in Figure 3, namely optical (1D and 2D images), and through the use of Langmuir probes. Even so the resultant blob/filament velocities tend to be of order a few percent of the local ion sound speed across an assortment of machine sizes and types (spherical tokamak, or ST, vs tokamak vs linear machine). While some experiments find a correlation of filament cross-section size with velocity, leading to larger and faster blobs near the separatrix [30, 37, 32, 15], there is also evidence that the filaments can have constant velocities in the SOL [35]. The large variation in normalized filament cross-section size seen in Fig. 3 is probably not due to differences in measurement techniques used: 1) At least three sets of size data (NSTX, MAST, C-Mod) are inferred from images; and 2) the ST data strongly correlate, as they should. There may be too strong a field dependence in the normalization (ρ_s) used which would be consistent with the lack of blob velocity or size

dependence on magnetic field in a single machine [31]. When the normalization of the data of Figure 3 is changed to that suggested by Myra (a*, v* [38]) the general scatter in Figure 3 is similar. However, if some adjustment is made for the filament length being shorter in spherical tokamaks then the ST results move closer to the other tokamaks.

There has been significant work investigating the relationship of the measured turbulence to the underlying physical processes. For example experimental measurements of the 2D potential and density distribution in the SOL show that the electric field of the turbulence-induced dipole structure is oriented such that the resulting ExB drift points radially outwards [35]. This finding is consistent with the basic models for radial propagation of fluctuation structures and suggests that this propagation is caused predominantly by curvature (although this is obviously not true for the linear machines).

There are several recent review papers detailing experimental, theoretical and modelling work in this area [39-41]. Some models have had success matching measured statistics and turbulence characteristics (e.g. size and velocity) [42, 31, 38]. In the most recent work comparing the electrostatic code ESEL with TCV [17, 43] and JET far SOL data [44] the model matched some of the turbulence characteristics but also the resultant SOL density profiles. The different experimental scalings of local plasma characteristics described earlier for the near (dependent on local pressure gradients) and far SOL (independent of local parameters) imply that different regions of the SOL appear to be governed by different processes. Those dependencies could be interpreted as due to electromagnetic effects in the near SOL where β is highest [4] and electrostatic effects in the far SOL [17, 43].

Inclusion of an approximation of such turbulent transport into predictive, fluid models of the divertor and SOL is being addressed at various levels. These include characterizing the time-averaged transport with spatially varying transport coefficients, usually including convection, the characteristics of which are deduced from experimental data or turbulent simulations. For the majority hydrogenic species, the convection is assumed, based on experiment [28, 18], to increase rapidly between the separatrix and the chamber wall giving a strong outward flux [45, 46]. Impurity transport is less well characterized, but arguments and modeling using a combination of outward and inward convection depending on the charge state have been presented [45]. To obtain direct information from turbulence for transport modeling, more detailed coupled simulations have been reported [46] where the turbulent hydrogenic fluxes are averaged over a time window of adjustable duration. These

approaches that use either fixed, time-averaged transport coefficients, or turbulent fluxes partially averaged over a time window, may miss significant details related to strongly intermittent processes (depending on the time-window size) for the highly nonlinear SOL transport response.

Parallel flows in the SOL play an important role in impurity transport, ideally sweeping impurities to the divertor before they can diffuse into the core plasma. Flows also play a central role in the co-deposition of D with carbon in present day tokamaks and are associated with concerns for T retention in ITER [23, 47]. Collecting Mach probe measurements from a number of divertor tokamaks, we find a fairly consistent flow pattern between divertors (Fig. 4) where all cases are with BxVB towards the lower divertor (lower, single-null plasma). The flows appear to reverse direction in the region between the low-field side midplane and the outer divertor. The flows also approach Mach 1 in the SOL at the high-field side midplane. This level of flow asymmetry between the low- and high-field SOLs is stronger than would be expected from fluid code modelling including drifts which, for example, predict that the Mach number should be highest at the midplane at the high- and low-field SOLs (due to Pfirsch-Schlutter flows). It has been proposed that the strong radial ballooning transport across the separatrix at the low-field side drives a poloidal pressure imbalance in the SOL which, in turn, drives flows along B to the inner edge [48, 49, 43], indicates that such pressure-driven flows add to and, in some locations, dominate drift effects (e.g. at the top of the machine with BxVB down [50]). The support for this pressure-driven flow hypothesis comes from several sources; First, high-field SOL probe measurements from C-Mod have demonstrated a pressure imbalance with respect to the low-field SOL consistent with that needed to drive flows [48]. Secondly, probe measurements at the top of the limiter tokamak Tore Supra, made while shifting the recycling limiter intersection poloidally, show the same poloidal flow imbalance as in divertor tokamaks [49]. This greatly strengthens the credibility of the proposed pressure imbalance model while at the same time demonstrating that the effect is independent of the existence of a separatrix. Lastly, low-field side Mach flow profile

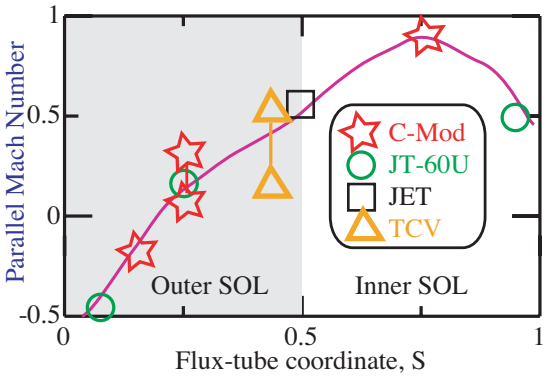

Figure 4: Parallel flow measurements in the SOL made by Langmuir probes at a number of points from the inner to outer divertor. S ranges from 0 at the outer divertor to 1 at the inner divertor. Positive Mach number (flow) corresponds to flow towards the inner

measurements from TCV evidence a field-direction independent component consistent in magnitude and direction with the enhanced low-field side radial transport and resultant pressure imbalance discussed above ([51] and references to similar profile measurements therein).

A further connection between low-field side transport and parallel flows is indicated through studies of turbulence. Langmuir probe measurements of SOL turbulence have shown a dynamical relationship between transport and parallel flows; As the size of the radial transport events increases, parallel flows also increase [52].

We note that any steady state flow of particles to the high-field side along field lines must be balanced by a returning flow across the LCFS, into the core and back to the low-field side again. Such a current could be carried by either ions (pinch) or neutral ionization. Experimental verification of such a process has not yet been made.

3. Edge Localized Modes (ELMs)

While the general transport discussed above generates steady state heat loads on PFC surfaces ELMs deposit large amounts of energy in a short time, and in some cases in a toroidally-localized fashion, that can lead to strong excursions in PFC surface temperatures. While the majority of ELM energy is deposited on divertor surfaces a significant fraction is carried to surfaces outside the divertor. There are obvious concerns that ELMs will lead to material erosion and reduced PFC lifetime. An additional concern is that even without erosion, thermal shock can lead to degradation of material thermo-mechanical properties. An example of such damage is that the ductility of the PFC (such as tungsten) is reduced leading to an enhanced probability of mechanical failure or spalling (erosion).

There has been considerable effort to characterize the ELMs in the SOL: Toroidal mode numbers are typically in the range n~2-20 [53-55], similar to the mode structure from stability analysis at ELM onset. The ELMs initially rotate toroidally (and poloidally) at high velocities (10s of km/s), similar to that of the main plasma. In MAST plasmas visible images show that the ELM toroidal rotation slows after 10's of microseconds simultaneous with a radial acceleration [56, 57]. Analysis of the divertor target power load pattern during ELMs in ASDEX-Upgrade also indicates that the toroidal rotation of ELMs is largely suppressed as the ELM propagates radially across the SOL [53].

Similar to the compilation of turbulent blob filament characteristics discussed above in Section 2 we have abstracted the physical size and velocity of the ELM filaments from published data [58, 59, 56, 60, 57, 55, 61, 62], all normalized to their respective pedestal ρ_s and c_s, Fig. 5. The scatter in both ELM filament size and velocity is potentially due to a host of variables including type of ELM, ELM energy, local plasma parameters, and the disparate measurement techniques (from Langmuir probes to image analysis). Radial velocities vary widely across devices (0.5 – 8 km/s), as well as within a single device (e.g. [59, 37, 56]). The range in measured ELM filament sizes is also quite wide - radial widths vary from 5 mm [62] up to 5-10 cm [56, 55, 61]. There is evidence that the filament cross-section is not circular; Based on toroidal images of filaments from C-Mod and NSTX [55, 62] radial widths are ~ 5mm and 30mm respectively while the respective poloidal lengths are a factor of 3-5 times larger. In contrast to turbulence blob/filaments the three experiments utilizing imaging techniques (Alcator C-Mod, MAST, NSTX) infer ELM filament sizes that, when normalized to ρ_s, are fairly well grouped. ρ_s may be a reasonable scaling parameter for ELM size.

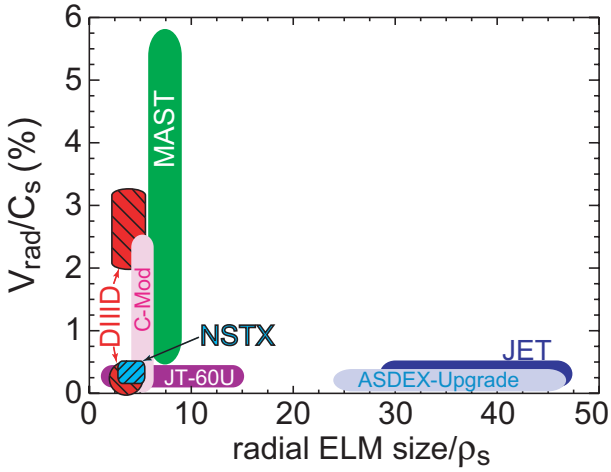

Figure 5: Radial cross-section size and radial velocity of ELM filaments in the SOL normalized to the ion Larmor radius at the electron temperature, ρ_s, and the ion sound speed, c_s for a variety of devices (see text). The normalization quantities are evaluated for pedestal parameters.

The initial period while the ELM is strongly rotating toroidally is also the period when most of the ELM energy is lost to the divertor (~80-90% of the overall ELM energy loss). New detailed measurements of the divertor ELM power flux have confirmed that the timescale for the ELM divertor power flux rise (similar to that of the ELM temperature rise time) is correlated with the parallel ion transport timescale, in good agreement with expectations from modeling [63-65]. On the basis of this, the power flux rise time for ITER is expected to be in the region of 250-500 μs. Figure 6 shows that during this time interval typically less than 30% of the total ELM divertor energy flux reaches the divertor target [66, 67], the remaining arriving in a time interval typically three times longer than that of the power rise time. Compared to previous estimates of power loading based on a square-wave power-flux waveform [1], the new predictions of the ELM power deposition time dependence decreases

the expected divertor surface temperature rise in ITER following an ELM of given magnitude and duration and the corresponding expected erosion [68, 69].

The divertor heat load pattern during the initial period when the ELM is rotating is similar in width to that between ELMs. In order to reconcile this toroidal uniformity with the ELM's toroidally-discrete nature one can invoke enhanced cross-field energy diffusion or field line ergodisation/stochasticity (e.g. [70, 71]) near the X-point. An additional effect is the toroidal rotation of the ELM which would tend to smear out any localized effects [68].

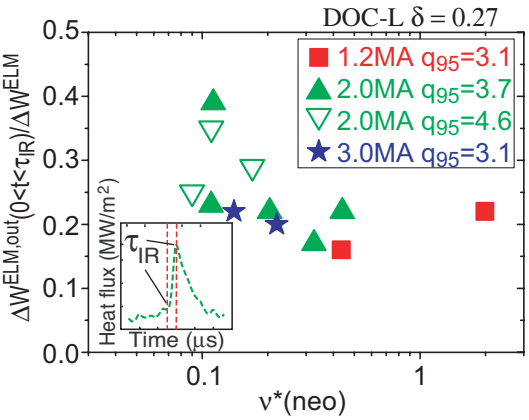

Figure 6: Proportion of the ELM energy arriving at the divertor in the time interval $[0,\tau_{IR}]$ (i.e. ELM start to the time of maximum power flux as shown in the inset) with respect to the total ELM divertor energy versus pedestal collisionality for a range of Type I ELMy H-modes at JET.

Careful analysis of infra-red thermographic ELM heat loads observed in the JET MarkIISRP and ASDEX-Upgrade Div IIb divertors has revealed an asymmetry in divertor heat loads (2:1) favouring the inner target for normal toroidal field direction (ion B$\times\nabla$B drift towards the X-point in lower single-null discharges) [51, 65]. This asymmetry is opposite to the behaviour in L-mode or inter-ELM H-mode JET plasmas [72]. While data exist only for a small number of reversed-field discharges in JET and ASDEX-Upgrade plasmas with low ELM energies, they show that that the ELM energy deposition asymmetry also reverses [65]. These trends are not yet explained. But it is clear from ASDEX-Upgrade that the ELM energy asymmetry is well-correlated with the passage of net charge from one target to the other [65]. These currents reverse direction with field reversal and there is no net current flow when the ELM energy loads to the targets are in balance (independent of the full ELM energy on the target). Under the assumption that the plasma temperature asymmetry, which drives thermoelectric currents, correlates with the power asymmetry (higher power flow to the outer divertor plate results in higher T_e there) then when the power asymmetry reverses during an ELM, the current asymmetry should as well. Since the current asymmetry does not reverse during ELMs and, if fact, increases in value, the currents are believed not to be thermoelectric in origin, in contrast to the inter-ELM current flow [65].

In contrast to the relatively smooth ELM heat load profiles peaked near the divertor strike-point which are observed as the ELM is toroidally rotating (discussed above), the loss of

energy to the divertor during the ELM's radial propagation away from the separatrix, combined with the toroidal mode structure of the filaments discussed above, is evident in heat flux striations outboard of the divertor strike-point [71]. The heat loads corresponding to such striations are much lower than for the main ELM heat load deposited earlier in the ELM lifetime.

Eventually the ELM's radial trajectory leads it to impact surfaces outside the divertor. At that point the filaments can still carry a significant fraction of the total ELM energy, typically in the range of 10-20% [73, 57]. Such convected fluxes are also predicted for typical medium Type I ELMs on JET using a recent model of ELM filament parallel particle and energy loss [67]. Extrapolation to ITER based on this model gives similar fractions of type I ELM energy delivered to main chamber PFCs [67]. Both model and JET experiments indicate that ions cool more slowly than electrons in the filament (through parallel losses) as it travels across the SOL [74]. Of course high T_i ions impacting main chamber PFCs are a concern since this enhances physical sputtering and impurity influxes, the level of which is dependent on PFC material choices there [23, 47]. Even with toroidal mode numbers of order 10 each individual filament carries ~1% of the total ELM energy and can lead to localized heat loading over small areas (10-20 cm^2) [73] of toroidally-discontinuous PFCs in a very short period, 100-200 μsec. Averaged over a number of ELMs, the ELM-derived deposited heat flux has a more poloidally-continuous profile over main chamber PFCs near the outer equatorial midplane [73]. Given the concentration of energy at the divertor during the ELM and the large flux expansion of the field lines near the upper X-point region in ITER (closest PFCs to the separatrix), the erosion of PFCs by ELMs is more critical for the lower divertor target than the first wall components (assuming that tile edges exposed to ELM fluxes are avoided in ITER). Instead, the impact of ELMs on main chamber PFCs is worrisome as a source of impurities which have a much higher probability of reaching the core plasma when born in the main chamber compared to that originating from the divertor [75, 25, 23].

The particle flux carried by ELMs to main chamber surfaces appears to be dependent on core plasma density and the energy per ELM. During low-density DIII-D H-modes (typically larger energy Type I ELMs), and with no external gas puffing, 80% of the particle flux to the outboard midplane limiter arrives during ELMs, even though the ELM duration is a small fraction of the time between ELMs [15]. At high density the fraction of limiter

particle flux occurring during ELMs remains high at 50% even though the ELMs are smaller and the radial ion flux between ELMs becomes much larger.

Early in the modelling of ITER performance Type I ELM heat loads were recognized to lead to a significant fraction of the overall ITER divertor erosion rate and thus limits PFC lifetime [76, 68, 3]. Recent modelling and experiments aimed at better understanding the effect of such transient heat loads on ITER-like materials and geometry have shown that the erosion and damage incurred is more than expected from the basic physical properties of the materials [77, 78]. For the case of Carbon Fiber Composite (CFC) graphite there is enhanced erosion along so-called PAN fibers oriented parallel to the surface; Such fibers have poorer heat conduction into the bulk leading to higher temperature excursions and faster sublimation (x10) than fibers oriented perpendicular to the surface (and whose properties have been used to predict tile lifetime in ITER). As a result of enhanced PAN fiber loss the effective heat-load handling area of the surface is diminished along with the capability of the surface to handle subsequent ELMs and disruptions. The results for similar tests of tungsten tiles [77, 78] showed enhanced erosion of the surface due to droplet formation and loss beyond what would be expected based just on evaporation. In addition, cracks were formed, some of which extend 0.5 mm into the surface. For both tungsten and CFCs such erosion leads to the rapid formation of dust which is a concern for safety and T retention (large surface area) in ITER [79].

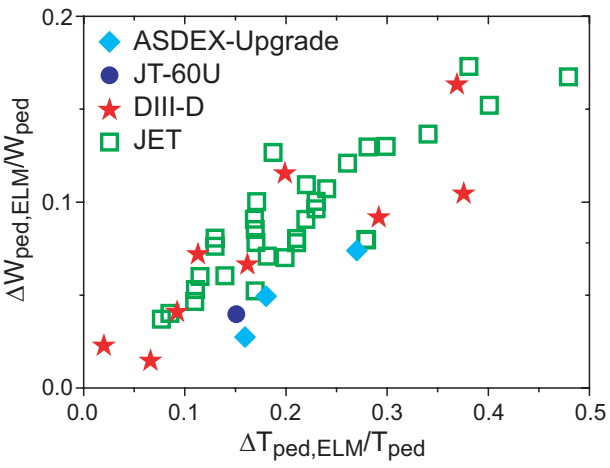

Figure 7. Normalised ELM energy drop versus normalised ELM temperature drop for a range of JET (low/high triangularity, q_{95} = 2.8 - 4.5 and forward and reversed field [80]), DIII-D [70], JT-60U [66] and ASDEX-Upgrade Type I ELMy H-modes [143] showing the correlation between small ELM energy losses and convective ELMs (small temperature drop).

Given the damage that ELMs present for ITER the question arises as to whether there is some ITER operating regime where the ELM energy release is reduced to a level more compatible with a divertor PFC lifetime of years. Fig. 7 shows that the magnitude of the ELM energy loss during Type I ELMs (ΔW_{ELM}) in a number of divertor tokamaks is dependent on the change of pedestal temperature at the ELM [68, 69]. Thus, Type I ELMs with small (normalised to the pedestal energy W_{ped} = 3 $n_{e,ped} T_{e,ped}$ V_{plasma}) energy losses

($\Delta W_{ELM}/W_{ped} < 0.05$) are associated with small changes of pedestal plasma temperature at the ELM, ΔT_{ELM} (typically $\Delta T_{ELM}/T_{ped} < 0.15$). In such cases convection dominates the transport of energy from the confined plasma onto open field lines. The achievement of small "convective" Type I ELMs for 'standard' operation in present tokamaks is associated with high density AND high collisionality operation [80]. This is at odds with what is needed for ITER to achieve small Type I ELM energy losses, namely high density (normalised to the Greenwald limit) and LOW collisionality conditions. Recent experiments at JET [80] and JT-60U [66] have shown that convective ELMs can also be achieved in low ν^* conditions. However, the plasma conditions which are required to access this ELM regime are not compatible with the requirements for Q_{DT} =10 operation in ITER, either because of the need for high q_{95} (~ 4.5) or the strong deterioration of plasma energy confinement as density is increased to achieve $<n_e> \sim 0.85 n_{GW}$. Experiments are underway to understand the interplay between the achievement of convective ELMs, global energy confinement and accessibility to high densities in order to bring these regimes closer to ITER's requirements.

Summarising the ELM results we conclude that type I ELM energy deposition represents a serious concern for ITER. The high instantaneous heat flux to divertor PFCs leads to erosion and reduction of the heat-load bearing capability of the surfaces that will limit divertor lifetime. Such a situation is unacceptable for routine ITER operation with Type I ELMs. $\Delta W_{ELM}/W_{ped}$ needs to be kept below 0.05 to maximize divertor lifetime. These concerns add renewed emphasis on identification and implementation of small ELM regimes and control techniques; Examples are pellet pacing, which reduces the energy released/ELM [81], and application of external magnetic perturbations to the pedestal region [82]. If we assume that regimes with tolerable ELMs for the divertor compatible with the required ITER performance are identified, the situation for PFC surfaces outside the divertor in ITER is less an issue of lifetime than of enhanced impurity sources in a region where the probability of reaching the core plasma is higher.

4. Disruptions

The energy fluxes and the ensuing damage as a result of the rapid energy deposition during disruptions is a large concern for the ITER PFC's. ITER has significantly higher (~x10) stored energy density normalized to total PFC surface area than present devices. Given that disruption thermal quench times (~ ms) are relatively insensitive to machine size the resultant large surface temperature rise can cause transient overheating damage to PFC surfaces, threatening their long-term viability for power handling. Additionally, ITER presently employs three different PFC materials at various locations and each material will respond differently to the energy pulse, particularly with regard to erosion (melting of Be or W versus sublimation of carbon) and the power threshold for significant losses (Be having a much lower melting temperature). Previously, it was assumed that most of the thermal energy deposition would be to the divertor region. However, measured energy deposition during disruptions at first-wall regions outside of the divertor can reach as high as 50% of the pre-disruption thermal and magnetic plasma energy [3]. This high heat flux is linked to two effects: 1) the broadening of the divertor heat load footprint by up to a factor of 10 during the MHD-induced thermal quench in divertor tokamaks as shown in Fig. 8 [83], and 2) an isotropic deposition of poloidal magnetic energy due to radiation in the current quench when the plasma is typically cold (T < 10 eV). A further mitigating factor for divertor heat loads is displayed in Figure 9; The fraction of thermal energy arriving on divertor surfaces during disruptions appears to be reduced on average as the stored thermal energy density in the plasma increases. These new insights lessen concerns that the divertor must absorb all the thermal energy of the plasma over a small area of the target. On the other hand there is more power flow to main chamber PFCs which may be less suited to deal with such rapid energy deposition.

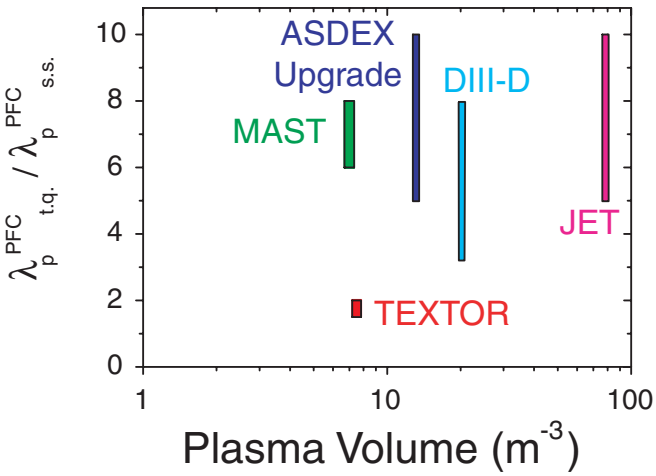

Figure 8: Ratio of the divertor power flux width at the thermal quench to that during steady state plasma conditions for various tokamak devices, showing the large broadening of the power flux width in divertor tokamaks, which is absent in limiter tokamaks.

Comparison of measurements from several divertor tokamaks has also yielded the insight that for many types of disruptions the plasma thermal energy content is often reduced as the disruption approaches. A clear example is that of density limit disruptions in which, prior to the thermal quench, degradation in energy confinement (e.g. reversion to L-mode) and the increase of plasma radiation (i.e. MARFE) have considerably reduced the stored energy. This behavior is shown in Fig. 10 for JET and ASDEX Upgrade [68, 69], a positive development for the survivability of all ITER PFCs to disruption loads. It is not clear at present if the lower disruption plasma energy measured at JET is due to a favourable size scaling or to disruption amelioration actions, which are applied routinely at JET but not in ASDEX-Upgrade.

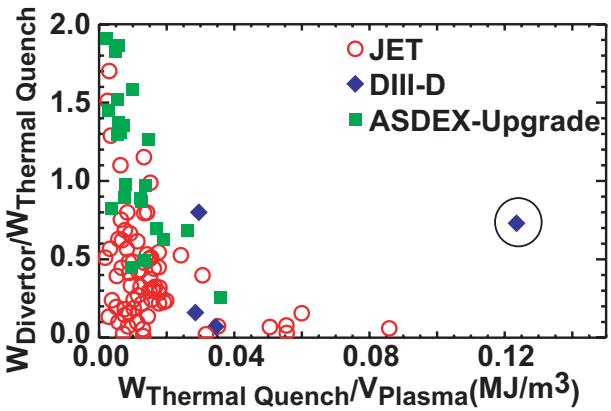

Figure 9: Ratio of plasma energy reaching the divertor to the total plasma thermal energy (at the thermal quench) plotted vs thermal quench energy (normalized by plasma volume). The circled point corresponds to a disruption of a discharge with an ITB.

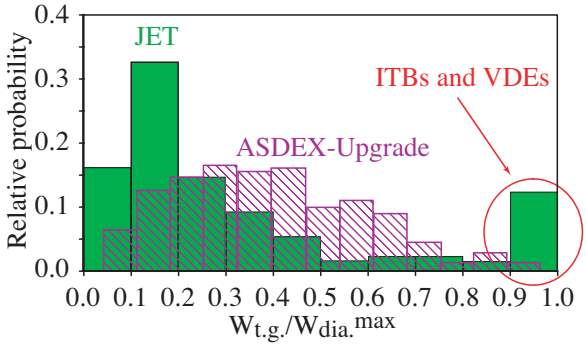

Figure 10. Relative probability for the fraction of disruption thermal energy in JET and ASDEX-Upgrade for a database of high-energy disruptive discharges.

As a consequence of the pre-disruption decrease of τ_E, increased power fluxes (to the divertor mostly) are measured in advance of the disruption thermal quench. In general, the timescale of these fluxes is longer than the energy confinement time and thus the surface temperature increases are of low magnitude compared to those at the thermal quench. Only when fast phenomena are involved, such as a growth of MHD modes with subsequent locking (toroidal rotation slowed to zero), and fast H-L transitions, can the pre-disruptive divertor power fluxes be significant compared to the thermal quench. This is in part due to the lack of a significant broadening of the power flux footprint during these transitions, contrary to the observations during the thermal quench [84]. In such fast transients the plasma can deposit an amount of energy in the range of 10-50% of that at full performance in timescales typically a factor of 5-10 smaller than the full-performance τ_E, as seen in JET and MAST. On the basis of these measurements, for most disruptions, the pre-

disruptive power flux transients are not expected to cause a significant erosion of the divertor target.

The exceptions to the pre-disruptive energy confinement deterioration behaviour (examples circled in Figures 9 and 10) are disruptions triggered by ideal-like β limits, such as for ITB (Internal Transport Barrier) plasmas, and disruptions caused by a Vertical Displacement Event (VDE) [68, 69]. In these cases there is no significant reduction in the plasma thermal energy before the disruption, which makes these disruption types of the highest concern for ITER operations. ITB-type disruptions in JET tend to have low fractional dissipation in the divertor, while for ideal-like β limits in DIII-D most of the thermal plasma energy is seen to flow to the divertor. On the other hand, the pure VDE disruptions typically lose their thermal energy to the area of contact between wall and plasma determined by the vertical movement of the plasma (frequently the PFCs outside the divertor area or main-wall). Therefore, any strategy to mitigate the disruptions so that the damage produced by thermal loads on PFCs is minimized should be adapted to the various disruption types.

Disruption mitigation techniques are being developed and tested in order to alleviate thermal and electromagnetic damage to PFCs on a variety of tokamaks with positive implications for ITER. Massive gas injection (injection of a number of particles similar to, or greater, than the target plasma inventory) is used on many tokamaks to mitigate disruptions by initiating a plasma quench dominated by impurity radiation. The duration of the thermal quench (TQ), i.e. the time required for the plasma thermal stored energy to be dissipated, is a key issue for PFC surfaces. Ideally the TQ is tailored by the impurity injection such that it is faster than the un-mitigated disruption, and therefore alleviates possible damage caused by plasma heat conduction to the wall. On the other hand the injection must not be so rapid that the radiation flash heats the wall PFC surfaces past their melting point, e.g. the beryllium main wall PFC in ITER. Fig. 11 shows TQ durations ~ 1-10 ms for noble gas disruption mitigation for ASDEX-Upgrade, DIII-D

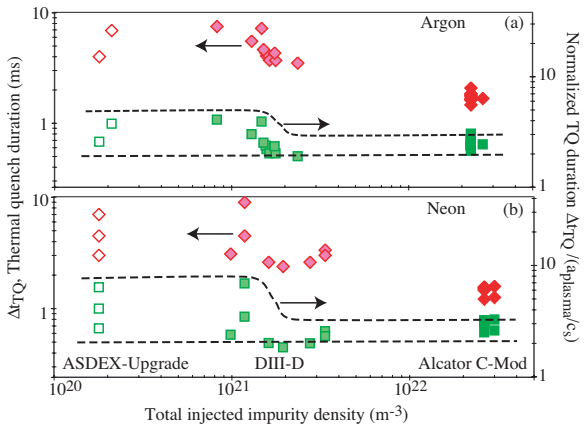

Figure 11: Thermal quench (TQ) duration for mitigated disruptions versus total injected impurity density of noble gas for a) argon and b) neon on ASDEX-Upgrade, DIII-D and Alcator C-Mod. Also shown is the TQ duration normalized to a/c_s the ratio of the plasma minor radius, a to the gas sound speed at room temperature, c_s.

and Alcator C-Mod. The TQ duration is measured as the time between the first diagnosis of edge plasma cooling or radiation, and the beginning of the current decay (however this does not guarantee that the radiated power is constant over this time). The differences in injection density arise from varying gas injection hardware and the small size/volume of C-Mod (a/V~0.2m/1m^3) versus AUG/DIII-D (a/V~ 0.6m/15m^3). The significantly faster TQ of C-Mod suggests a size dependence, whilst the fastest TQ times of DIII-D and AUG, which are nearly of identical size, are similar despite large differences in injected density. The generally faster TQ times of neon compared to argon further suggest that the less massive impurities induce the radiative quench more quickly, in a manner similar to the more rapid transit time of the gas from reservoir to the plasma edge [85]. Based on these observations, it is found that the fastest TQ durations are well organized by normalizing (square symbols in Fig. 11) to the transit time of the gas across the plasma size, a/c_s, where c_s is the gas sound speed at room temperature which varies with the gas atomic weight as $1/M^{1/2}$. This simple size and gas mass scaling appears sufficient despite the fact that is now understood that the gas does not penetrate ballistically through the plasma during the TQ [86, 87], therefore suggesting a process linked to the transport time of ionized impurities in the plasma. The details of the TQ are complicated by the MHD effects induced by the impurity cooling in the edge plasma [88] which suggest radial impurity penetration via island formation and field-line stochasticity. The role of MHD in setting the TQ timescale remains uncertain and is the subject of ongoing numerical modeling. The TQ time is consistently found at its minimum values (i.e. less scatter) when the injected impurity density exceeds $2x10^{21}$ m^{-3}, suggesting a threshold for obtaining reproducible TQ durations. Using the simple empirical size scaling suggested by Figure 11, the induced TQ time of ITER is ~ 9-24 ms using pure neon injection. Such time scales are longer than predicted by 0-D modeling ~1 ms [89]. If the radiation release time in ITER resulting from massive gas injection also followed the above empirical size scaling then it would not lead to melting of the beryllium first wall. However significantly slower induced TQ durations (> 20 ms) may be too slow to mitigate the fastest types of disruptions on ITER (e.g. with ITBs), when the finite delivery time of the neon gas (~10-20 ms) to the plasma edge is taken into account. Further experiments (e.g. on JET) and modeling are required to understand the phenomena controlling the TQ duration.

5. Tritium retention

The retention of tritium is a serious concern for ITER given that 50g is to be injected each full-power D-T discharge and the in-vessel limit may be as low as 330g [1]. Our current working premise for D or T retention in existing carbon-PFC tokamaks is that hydrogenic retention is dominated by co-deposition with carbon forming hydrogen-rich carbon surface layers. An important erosion source of the carbon appears to be due to plasma contact with main chamber surfaces with resultant chemical- and physical-sputtering. The eroded carbon is then transported to the inner divertor in the strong SOL flows described in section 2 resulting in a nearly universal pattern of inner divertor net carbon deposition in present tokamaks [23, 47]. Once the carbon reaches, and is deposited on the inner divertor, it can be transported further by local re-erosion (due to steady-state ion fluxes or ELMs) and by volume recombination from the C^{+1} state [90], until finally the C (and co-deposited D) cannot be eroded further, having come to rest on surfaces facing low-T_e plasmas and areas shadowed from direct plasma contact where the erosion is weak (compared to the deposition rate). It is likely that ELMs play an important role in the last erosion steps at the inner divertor, by their ability to erode C through sputtering, sublimation and thermal transients. The latter erosion process could, in principle, launch clusters of C from the surface (dust), which, along with the flux of C atoms resulting from C^{+1} recombination, would potentially explain the co-deposition of C and D at surface locations in the private flux region or other surfaces that view the strike-point region; The charge exchange mean free paths of chemically sputtered molecules should not permit them to make it through the divertor leg without ionization whilst clusters have long mean free paths since they are stopped by ablation processes as opposed to ionization.

Present global hydrogenic retention fractions of the injected fuel for pulse-lengths of order seconds are in the range of 3 to 30% [91-93, 3]. The lower range of retention fractions are typically based on post-campaign analysis of individual tiles (exposed to an entire campaign of discharges) using ion beam techniques. Such techniques, which have been successfully applied to tiles from most operating tokamaks, probably underestimate fuel retention in an individual discharge as they integrate over multiple events that lead to D outgassing such as disruptions and cleanings that occur during a run campaign. Moreover, in general, only a small fraction of PFC surfaces are typically analyzed (e.g. a sampling at one toroidal location at many points poloidally) and results are extrapolated assuming toroidal symmetry. The higher levels of retention cited above are inferred from global gas balance measurements which rely on single discharge integrations of the difference between injected

and pumped gas. However, the database of global particle balance is still limited and suffers also from limited accuracy of the measurements. These measurements are likely over-estimating fuel retention because gas release due to the occasional disruption, or occurring slowly over long periods between discharges (e.g. nights, weekends) is not included. The current H and D retention fraction database (3-30%) with carbon-PFC dominated machines has been extrapolated to ITER giving a range of T retention between 1.6 and 27 g/shot [3]. The large range reflects the uncertainties in current measurements and the lack of understanding of how to properly extrapolate such results to ITER. It does not reflect the fact that ITER will be operating with a different mix of materials/temperatures than present devices. Efforts to model the effect of replacing C with Be over 90% of the PFC surfaces have resulted in a slight reduction (factor of 2) in the maximum T retention rate with the ITER vessel limit for T reached after 55-140 full power discharges [94, 95]. In any case the high levels of retention and corresponding uncertainties indicates the need for a significant tritium removal capability. Overall, D retention in tokamaks with high-Z PFCs appears lower than for carbon, but still higher than scaled from previous non-tokamak, or laboratory, experiments [3, 96].

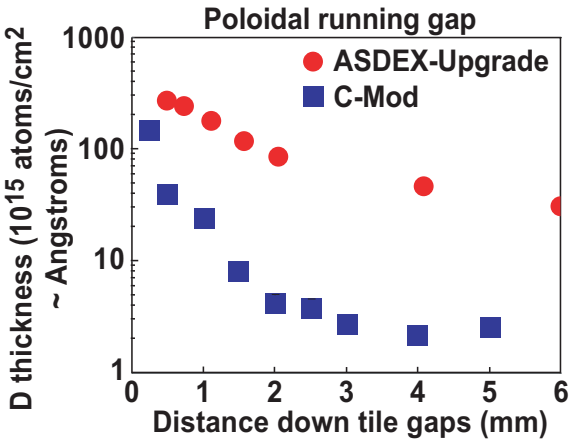

Figure 12: D retention on tile sides between 2 toroidally-adjacent tiles. The ASDEX-Upgrade data [99] is from C tiles with a gap of 0.5-1 mm between them and an ion fluence of 5×10^{23} m^2 (17 s of discharge time). The gap size for C-Mod is 0.5 mm and corresponding ion fluence is 1.56×10^{26} m^2 (campaign averaged over 5500 seconds). The D inventory in deposits was measured by Nuclear Reaction Analysis using the reaction D(^{3}He,H)^{4}He

One area of efforts in the ITPA research community to understand and characterize the global gas retention in PFC surfaces has been the investigation of the level of D retention on the sides of tiles (in gaps between PFCs) as well as the processes involved. The literature indicates that a large fraction (15-30%) of overall D/T retained is found on the sides of tiles [97, 98]. There are roughly 10^4 tiles in many of the currently-operating tokamaks while the ITER design utilizes approximately 10^6 castellated and macrobrush armour tiles. More importantly, while most current carbon PFC tiles have front to side area ratios in the range 1.25-2, ITER will have a surface area ratio closer to 0.7 thus increasing the relative level of side surface area, and potentially the relative contribution of tile sides to T retention. As will be discussed later T retention on tile sides is more difficult to remove than on the front surfaces. It is also important to

understand the processes that lead to tile side retention as that may lead to the capability to design tiles and/or change ITER operational characteristics in order to reduce that retention. A better understanding of D retention processes might also be used to optimize T removal techniques for those surfaces. For reference, in current high-Z PFC tokamaks the surface area ratio varies from ~ 2 (ASDEX-Upgrade) to 0.4 (C-Mod), the latter low value driven by a need to reduce eddy current induced forces in solid Mo in disruptions.

Through an ITPA-organized study of D retention on the sides of tiles that included multiple tokamaks we have found generally similar D retention profiles on the sides of tiles. Figure 12 displays an example of the typical falloff of D density with distance from the front surface of an ASDEX-Upgrade graphite tile [99] and a molybdenum one from C-Mod where the gaps (0.5 – 1.0 mm) are between 2 toroidally-adjacent tiles (poloidal gap). Note that the ion fluence to the C-Mod tile (front surface) is a factor of 500 larger than that to the ASDEX-upgrade tile. The e-folding length for drop in D density is typically 1-2x the gap size [100, 101, 99]. The e-folding length near the surface is often shorter than further into the gap [101, 99]. The obvious process in the D retention on tile sides is co-deposition of D with carbon in carbon PFC machines (In the C-Mod case the co-deposition of D is with boron, which is present due to boronization). This process also leads to a competing re-erosion of deposited carbon (or boron) by chemical erosion with atomic hydrogen. One model of the deposition is that C:D molecules (C_xD_y) eroded from the front surfaces or leading edges, are dissociated in front of the gap, with some resultant component parts of the original molecule headed down the gap. Alternatively, if there is direct ion flux to the leading edge of a particular tile, eroded C and C:D molecules can be directly deposited on tile sides. In either model the deposition profile is then determined by where the molecules/atoms originate and the sticking coefficients of fragments to surfaces as they impact tile sides. Preliminary modelling of the co-deposition process has been done [102, 103, 99].

The comparison of D deposition on the sides of tiles from high and low D^+ fluence regions shows generally that higher fluence regions (e.g. divertor) have higher tile-side retention (and C deposition). This is consistent with the hypothesis explaining the tile side retention discussed above. Higher ion fluxes to carbon tiles can generate a proportionately larger source of hydrocarbon molecules eroded in, or dissociating in front of, a tile gap, leading to increased co-deposition on tile sides. We also note that such a model for D retention on tiles sides implies that minimizing gap size and the tile side to front surface area would further

reduce tile side D/T retention. Furthermore, if the dominant tile-side deposition process is due to direct deposition following leading edge impact and erosion it may be possible to strongly reduce tile side retention by minimizing leading edges (top edge of tile side) by, for example, shadowing all leading edges from ion impact [104] Of course, minimizing the C (or Be) concentration in the high ion flux PFC regions will also reduce the erosion and subsequent co-deposition.

Minimization of D/T retention on the sides of tiles beyond the geometrical prescriptions described above can also be achieved through maximizing tile temperatures. Elevated surface temperatures above 200°C led to a reduction of the D-retention by a factor of 10 in a DIII-D gap retention study [99], an effect also observed for front surface deposition [105]. The reduction is assumed to originate from the temperature dependent re-erosion by thermal hydrogen atoms resulting in the emission of heavier hydrocarbon molecules [105, 99]. The cavity experiments at DIII-D indicate that most of these molecules have low sticking coefficients and escape the gaps without further deposition.

To test directly the hypothesis that tile side D retention scales with ion fluence to the front surface the multiple-tokamak database of retention information for 0.5mm gaps was re-analyzed and is shown in Fig. 13 (some data appears in another form in [100, 99]). D retention is ~ 1% of the ion flux to the corresponding front surface for carbon-PFC divertors while, for the fully high-Z PFC device included, the tile side retention is significantly lower. The lower retention rate for the Mo tile is also evident from Figure 12. Note that at the time of the ASDEX-Upgrade tile exposure a significant fraction of the tiles in the machine were manufactured from carbon as opposed to tungsten.

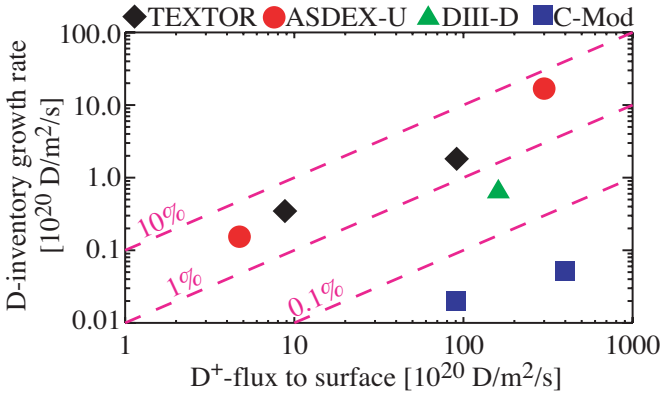

Figure 13: Tile side D retention rate dependence on front surface ion flux. Data are from carbon tiles (Mo in C-Mod) & boronized surfaces. All tiles used in this study had tile gaps of 0.5 mm. The tile side D growth rate is determined by integrating the total D inventory on the tile sides, and then dividing by the gap area (length of 4 sides x half the gap width) and exposure time. The ion flux to the front surface is just that perpendicular to the surface.

The much lower level of D retention fraction on tile sides observed in C-Mod with Mo PFCs occurs even though C-Mod tiles have a significantly higher ratio of side to front-

surface area than the carbon-PFC machines included in this study (about a factor of 5) which might lead to higher gap deposition. Since the co-deposition of D in C-Mod is with boron instead of carbon the implication is that the rates of several of the processes involved; DB (deuterium and boron molecule) chemical erosion, DB dissociation, and DB co-deposition, are much reduced compared to that for hydrocarbons (see, e.g., [106]). Note also that the C-Mod tiles utilized in this study had chamfered edges between toroidally-adjacent tiles to minimize, or eliminate, ion impact on leading edges.

The wealth of existing D and T retention operational experience described above is derived from short-pulse tokamaks. In recent years experiments on several long-pulse devices have revealed common long-pulse effects [107]: During the pulse, in a first phase (up till ~1s in JET [108] up to ~100s in Tore Supra [109]), the retention rate decreases, becoming constant in the following second phase. Although the D retention in the second phase can reach a significant fraction of the injected flux (50-80%) it represents only a small fraction of the recycling flux (1-5%).

There are long-pulse discharges where the gas retention rate can be low, or negative. In such discharges lower fuelling rates are used, such as long JET L-modes [108], or repetitive long H-modes performed in JT-60U [110]. In the latter case, where the walls are not actively-cooled, increases in surface temperatures lead to local outgassing which can dominate the plasma particle balance yielding, in turn, an increase in density.

An important characteristic of long-pulse Tore Supra discharges is that the amount of gas recovered after each discharge is independent of pulse length [109]. As a consequence the accumulated wall inventory is proportional to the discharge time or the fluence [111, 107]. A possible interpretation is that only D retained in the initial phase of the discharge is dynamically released between discharges. In practice, for Tore-Supra, this means that over a day of short discharges the integrated wall inventory stays below 10% of the injected gas and can be recovered from the walls by a night of glow discharge conditioning. In contrast, during a day of long discharges the gas recovery between discharges, or overnight, is negligible and

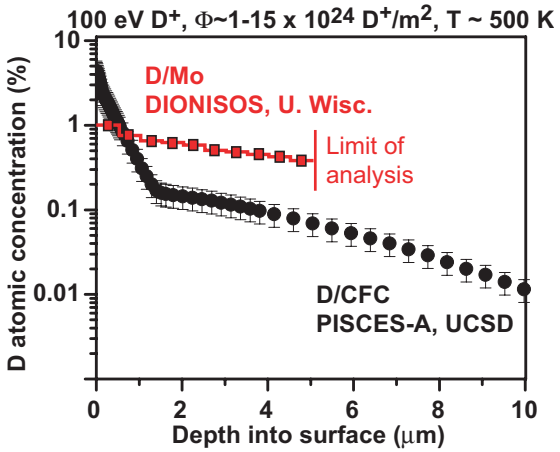

Figure 14: Depth profile of D within the surface of Mo and carbon CFC tiles.

the accumulated inventory can reach 50% of the injected gas. The retained fraction drops to of order 10-20% of the injected gas when integrated over a campaign that includes both long and short discharges [111], more similar to the results of short-pulse discharges discussed earlier in this section. At the moment the differences between long- and short-pulse gas retention are not well understood and are the subject of ongoing research due to its importance for a long-pulse ITER.

Recent results raise the possibility that deep diffusion/migration of D into the bulk PFC material is an important process to consider in D retention. Co-deposition of deuterium with carbon can explain the magnitude of long-pulse retention observed in the JET DTE1 campaign [111], but seems to be insufficient the measured retention for Tore Supra [107]. There are mixed results on whether co-deposition is sufficient or not to explain JT-60U retention results [112, 110]. Co-deposition is more clearly not responsible for the gas retention in Alcator C-Mod where 35-50% of the injected gas is retained after single, short discharges (1 second) with, or without B coatings on Mo tiles [113, 93, 114]. Laboratory experiments, coordinated through the ITPA, confirm deep penetration of D into CFC graphite [115] (over lengths of tens of microns) as well as in Mo [96] and W [116]. A comparison of the D profile within carbon and Mo tiles is given in Figure 14. The profiles typically have a sharper falloff near the surface with a slower e-folding into the bulk. Implantation of the D into the different materials was done using ion-beams (CFC and W) and plasmas (Mo). The results are surprising since the range of implanted D is of the order of nm. One would then not expect the D to be found in the bulk of either of these materials but rather concentrated near the surface. For carbon this is because the mobility of D in carbon is very low. While the diffusion of D in Mo is high there are normally no sites for the D to be trapped. Clearly, migration of D into the bulk of the material to depths of tens of micrometers is observed, either along grain boundaries or through interconnected porosity, before reaching stable trapping sites. We note that neutron damage (displacements of atoms throughout the bulk of the tile) to PFC materials in ITER and reactors will lead to additional sites for tritium to reside, the rate of site production linear in nuclear fluence.

The existence of substantial D inventory deep within tiles has the potential to impact the viability of tritium-removal methods to be used in ITER. To evaluate the relative contribution of co-deposition vs deep diffusion to D retention one needs to examine the scaling of the retention with ion fluence to PFC surfaces. D retention due to co-deposition scales linearly with the net deposition rate and therefore does not saturate. The initial

laboratory studies where D is implanted by ion beams indicate that the deep D retention in C and W scales with the square root of fluence indicative of a retention process that is limited by diffusion. The data for the scaling of D retention with fluence in Mo are more scattered: Laboratory experiments (ions implanted with plasmas) show retention scaling like the square root of fluence at 300°K climbing to a scaling like fluence for T > 400°K [96]. Experiments with C-Mod tokamak plasmas imply a scaling proportional to fluence which does not appear to saturate after ~ 30s cumulative plasma exposure (local ion flux perpendicular to the divertor surface in the range 1-10x10^{22}/m^2/s) [93]. Further studies of deep retention are required to better understand the process(es) involved, the differences among various PFC materials, whether the implantation of D by ion beams vs plasmas is different due to the larger particle flux density of the plasmas, and the importance of the role of neutron damage.

Given the large uncertainties in ITER T retention and the requirement to halt operation to remove T once the T inventory approaches 330g, it is clear that demonstrations of fast and efficient T removal techniques in contemporary tokamaks are required. Initial cleaning efforts on TFTR and JET were slow (~10^{-3} g/hour) [3]. Assuming of order 100 g of T needs to be removed overnight the required T removal rate would be ~ 10 g/hour. The methods currently being developed for removal of T from carbon fall loosely into 2 types [117, 118]: 1) heat the surface beyond 900°K such that the a-C:T bond is broken and the T liberated (scanning laser or radiative plasma termination) or; 2) remove the mixed C/T layer completely by ablation (heating using lasers or flash-lamps) or oxidation of re-deposited carbon layers. Although such techniques have not been tested widely the removal rates in some cases approach that needed for a strictly carbon PFC ITER [118, 119]. However, no single technique has been identified that would work with a mixture of materials. The above T recovery methods must be compatible with the ITER toroidal field, able to remove T from several materials and material mixtures, and not lead to additional problems (e.g. dust formation, corrosion of surfaces by T_20 or, through some way, compromise following discharges, for example, by raising oxygen levels). It is likely that no single T removal scheme will be sufficient and, depending on the retention rate, a combination of different methods will be applied at different times. If ITER PFCs that retain the highest fraction of T (e.g. the inner divertor and dome) could be heated to elevated temperatures (e.g. >200°C for Be, >400°C for C) the amount of T retained in PFCs could be substantially reduced leading to reduced need of T removal techniques.

The present ITER diagnostic complement does not allow assessment of the gas (H, D or T) retention occurring during, or even after a discharge. The capability of measuring H/D retention during the initial, non-activated, ITER operational phase (H, D) will be important in determining the optimal choice of PFC materials for the activated phase (T). The ITER team and the ITPA Diagnostic group are working to improve the diagnostic capability such that accurate measurements of injected and exhausted particles (H, D and T) can be carried out real-time during ITER discharges.

6. Materials

In contrast to current tokamaks ITER plans to have Be, C and W PFC surfaces, thereby minimizing C usage and, potentially, T retention. New studies indicate that such a mix of materials creates new effects: First, an intermixture of different material layers, alloys or compounds may be formed with strongly different thermo-mechanical properties. An example is that at higher temperature (800-1200°C) Be and W can alloy which leads to reduced melting temperatures (Be_2W: 2250°C, $Be_{12}W$: <1750°C, $Be_{22}W$: <1300°C) [120-122] thus reducing the heat load capability of the PFC surface or leading to higher erosion by melt layer loss. However, the formation of possible alloys does not occur under thermal equilibrium but is given by the Be-fluxes and the competition between Be sublimation, erosion and possible alloying. This indicates that the formation of thicker alloyed layers is minimized under divertor conditions where the heat loads are highest [26]. A second effect brought about by such a mix of materials is surface alloy and carbon compound formation (Be_2C, WC) which will also influence the tritium retention capabilities of metals [123, 124, 26]; Such surface compounds may retain more hydrogen than pure metals as indicated by some data, or even act as out-diffusion barriers for implanted hydrogen isotopes, thus increasing bulk retention or permeation. Lastly, modification of C surfaces through buildup of metal or carbide precipitates there (e.g. through simultaneous incidence of Be and D/T ions) can reduce carbon chemical erosion [125], a beneficial effect which will extend surface lifetime and also possibly reduce co-deposition of fuel with carbon. Carbon materials doped with metals typically show reduced chemical erosion yields [126] which

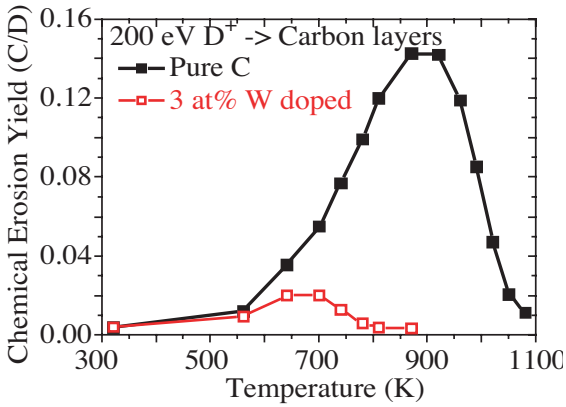

Figure 15: Temperature dependence of the chemical erosion of pure carbon compared to W-doped carbon layers [127].

may open additional possibilities to develop advanced graphite PFCs (Figure 15 [127]). Graphites doped with small additions of Ti, Si and B have been tested in tokamaks with both positive ([128] and references therein) and negative results [129]. Certainly material mixing gives rise to both potential risks and opportunities for plasma-wall interaction issues. Further studies are needed both in laboratory experiments and in fusion devices.

Most fusion reactor studies prefer tungsten over carbon due to its advantages with respect to erosion and neutron damage [130-132] as well as the level of tritium retention which is predicted to be lower by orders of magnitude [133] than with carbon PFCs. It is clear that prior to operation of any fully-ignited fusion reactor the compatibility of high-Z PFCs with high performance operation, without low-Z coatings, needs to be demonstrated in ITER. Recently, both Alcator C-Mod (entirely molybdenum PFC tiles) and ASDEX-Upgrade (most recently 85% W-coated carbon PFCs) have compared the compatibility of high-Z vs low-Z PFC surfaces for core plasma operation [113, 114, 134, 135]. Boronization can strongly lower the core concentration of W or Mo and medium Z impurities, lowering radiation in the core. If the boronization follows a machine opening where the walls are cleaned of B the drop in core concentration of Mo can be a factor of 100 [113]. Subsequent boronizations have a less dramatic, but still important, effect on core impurity levels as shown in Figure 16. In Alcator C-Mod the drop in core Mo concentration also improves the quality of H-modes. Experiments indicate that the erosion of the boron layers over a small fraction of the full PFC area leads to a rapid recovery of the core Mo/W levels back to pre-boronization equilibrium over 10's of shots (Figure 16). The erosion mechanism of B layers and the underlying high-Z surface during ICRF heating appears to be an RF enhancement of the surface sheath ('sheath-rectification') that then accelerates impurity ions (C^{4+}, B^{3+}) into surfaces leading to physical sputtering at the top of

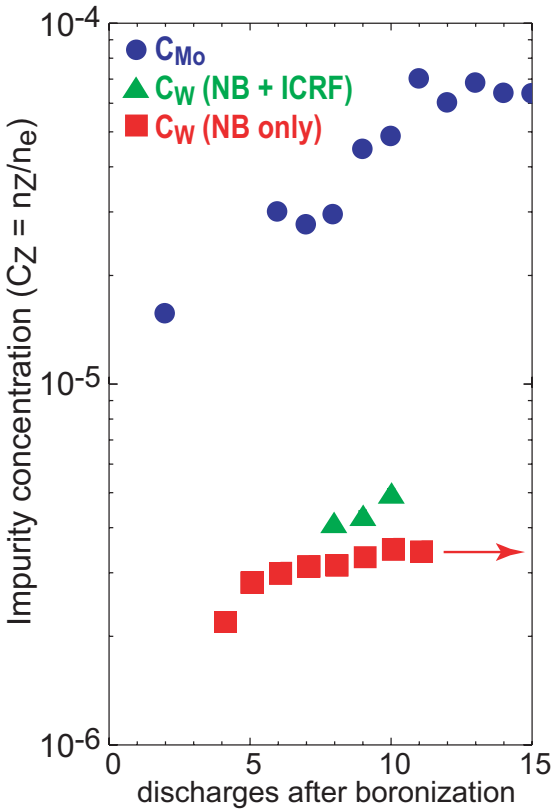

Figure 16: Recovery of core concentration of high-Z impurities following a boronization in C-Mod (3 MW ICRF, $n_e \sim 4x10^{20}$ m^{-3}), ASDEX-Upgrade (5-7.5 MW Neutral beam, $n_e \sim 6\text{-}8x10^{19}$ m^{-3}, squares) with 1-2 MW of additional ICRF power (triangles).

the outer divertor (C-Mod [113, 114]) and the ICRF guard limiters (ASDEX-Upgrade [134]). For NB-heated plasmas fast ions drift out of the core and impact the low-field side guard limiters again leading to W physical sputtering [136]. In general the B erosion, and subsequent W/Mo erosion, is faster for ICRF-heated plasmas as opposed to NB or Ohmic H-modes (Figure 16) [113, 114]. C-Mod results indicate that the tungsten planned for ITER is in a location that may be heavily eroded during ICRH-heated discharges (top of the divertor). ASDEX-Upgrade results raise concerns over a Be outer limiter in ITER in combination with ICRF. However, during NB-heated plasmas the W levels appear to be lower with less of an effect on the core plasma. Further experiments on the 2 tokamaks will clarify the physics underlying high-Z PFCs (and their coatings) as well as implications for a fully-W ITER. In addition, ASDEX-Upgrade is in the process of coating the last remaining carbon surfaces with tungsten thus converting to an all-W PFC surface tokamak. We also look forward to the change in JET PFCs to Be walls and a W divertor which will provide additional information on high-Z PFC operation as well as the interaction of Be with W in a tokamak environment [137].

7. The ITER divertor and collisional neutrals

In predicting ITER performance it is clear that we must have confidence that codes are able to predict accurately plasma performance in present devices. In earlier sections we have reviewed modelling efforts associated with combining turbulence models with steady state SOL profile predictions as well as the efforts to explain the dominance of flows along field lines towards the inner divertor. In the area of divertor modelling current plasma/neutral models have reproduced measured divertor pressures in the neutral kinetic regime common to most current tokamaks. However, there has been difficulty in matching experimental observations on Alcator C-Mod where neutrals are more fluid-like, a neutral transport regime predicted for the ITER divertor. Recent interpretive modelling efforts have employed the Onion Skin Model (OSM) - EIRENE combination where a number of new physics processes have been implemented – neutral viscosity, neutral-ion collisions, and Lyman-alpha photon trapping [138]. With these modifications, C-Mod's ITER-like neutral pressures and other divertor characteristics are more closely reproduced. While at the highest densities recombination is the source of 80% of the neutrals in the divertor, Lyman-alpha trapping has the potential to strongly reduce the recombination rate (photons re-ionize neutrals) and modify the detachment density threshold. The same code improvements have been included in the B2-EIRENE code [139, 140]. When the model is applied to ITER

nonlinear neutral effects cause the Private Flux Region neutral pressure operational range to shift to ~ 2x higher values [139] as compared to previous, linear neutral, studies. The introduction of divertor Lyman-alpha trapping, although modifying the local plasma parameters, did not affect the ITER divertor performance with respect to the power and particle handling [140]. The benchmarking of the new code physics against C-Mod as well as the continued testing for ITER [141] is ongoing.

In parallel with the above testing of the code physics against experiment a program of code-code benchmarking has been followed (EDGE2D to SOLPS to UEDGE [142, 46]). This process has brought to fore the different physics assumptions across codes (e.g. treatment of kinetic electrons, neutral and ion flux limiters, the Bohm Mach condition at the divertor surfaces and the treatment of drifts in the core plasma), some of which can lead to significant differences in the model output. Current plans are for more comparisons of the codes with impurities and drift processes turned on successively.

8. Summary

Recent advancements in measurements and modeling have considerably improved our understanding of the SOL and divertor physics needed to predict and maximize ITER performance. Studies of steady state profile characteristics of both the near and far SOL regions show progress in connecting observed profile characteristics to the underlying physics as well as developing empirical scaling of profile characteristics applicable to ITER. Measurements of the underlying turbulence characteristics show similarities across devices. Models of the turbulence in the SOL have matched characteristics of the measured turbulence and in one case, the steady state density profile. A new mechanism has been proposed to explain the strong SOL flows that have been observed, and which play such an important role in impurity transport and T co-deposition.

The characteristics of ELMs (e.g. size, toroidal and radial velocity) as they travel though the SOL have been much more clearly defined posing a significant challenge to modelers. Most of the ELM energy is transmitted to the divertor in an initial period (~ 50 μs) while the ELM filaments are rotating toroidally giving rise to a heat load profile that is similar in shape to the steady state profile, but with an in-out asymmetry peaked on the inner divertor for B$\times\nabla$B towards the divertor. 10-20% of the ELM energy is carried into the far SOL impacting the leading edges of the many surfaces there. The resultant impulse heat loads of

individual ELMs are very localized on main chamber PFCs while, over many ELMs, the heat loads are more uniform (at least near the midplane) similar to steady-state heat loads. While the ELM energy divertor energy deposition is most worrisome for PFC lifetime, our concerns over ELM loads to main chamber PFCs mainly relate to the impurity sources engendered. The time dependence of the divertor heat pulse during the first phase of the ELM is much different than the square-wave power pulse originally envisioned and used for modeling, spreading the power loading over a longer period. The newer measurements show that only about 30% of the divertor ELM heat load arrives over the short period that dominates the divertor temperature rise. That lowers the predictions for ITER divertor PFC surface temperature rise per ELM.

Transient power deposition estimates for disruptions have been lowered for the divertor, but raised for the main chamber. The heat load footprint to the divertor is up to 10x broader than the steady state heat load giving rise to power deposition outside the divertor. Main chamber disruption heat loads also include the uniform radiation that occurs during the current quench period as the magnetic energy is dissipated. Most disruptions that occur in current devices lose a significant fraction (up to 80%) of the thermal energy before the thermal quench. However, ITB disruptions and VDEs carry the full thermal energy into the disruption. Disruption mitigation utilizing massive gas injection has reduced the measured divertor loadings and probably can dissipate VDE disruptions in ITER before they release all their energy onto divertor and main chamber PFCs; VDE displacements in ITER are projected to be of order 0.1-1.0s, thus much greater than the thermal quench time whether induced or not [1]. It is more speculative to predict the efficacy of disruption mitigation with ITBs as they occur over faster timescales than VDEs. In any case, the general impurity radiation used to minimize divertor heat loads leads to increased main chamber loadings such that Be melting in ITER may be a concern.

Both tungsten and CFC graphite tiles have been tested under ITER conditions approximating ELMs and disruptions and the materials performed more poorly then predicted. Those CFC fibers oriented parallel to the surface fail to conduct the heat away and are then eroded up to a factor of 10 faster than would be expected from the average tile thermal conductivity assumed. The tungsten erosion, tested under the same conditions, was enhanced by droplet formation (leading to dust) and release.

Estimates of T retention have been reduced, but the level of T retention predicted for ITER will probably still mandate interruptions in operation to remove T. The D retention rate measured for present tokamaks as a fraction of injected gas, is primarily attributed to C co-deposition with D and extends over a wide range from 3-30%. Assuming Be is the dominant PFC material in ITER, models of impurity migration and D co-deposition predict that the retention rate drops by a factor of ~ 2 compared to the case of all C PFCs. The corresponding number of discharges before ITER operation would need to be stopped to remove retained T is then predicted to be in the range of 55-140 discharges. Tile side retention contributes a significant fraction of the overall T retention in current devices (~ 25%) and is most likely due to C erosion near, or at, the tile gap and subsequent co-deposition with D. The D or T retention rate on the sides of PFC tiles appears to be ~ a few % of the ion flux impacting the corresponding front surface for C tiles, but much lower for Mo. A number of possible control variables have been identified that might be used to reduce the retention of D on tile sides. These include geometrical changes (tile gap size, shadowing of tile gaps) as well as operation with heated tiles. The latter is also useful for D retention on any material surface. A number of T removal techniques are being developed with significant progress made for strictly carbon PFC surfaces. Depending on the T retention rate and principal retention locations a number of removal techniques will be needed at various times in ITER operation. The combined use of Be, W and C for ITER tiles should reduce T retention (through reduced T/Be ratios at lower temperatures than for all carbon PFCs), and has the potential to reduce chemical sputtering. However, mixed materials complicate T removal and also raise the potential for surface alloying (e.g. Be with W) accompanied by reductions in the surface melting temperature.

In summary, significant progress has been made in clarifying the SOL and divertor physics of ITER, but the basic problems of excessive first-wall power loading and tritium retention have yet to be solved.

References

[1] ITER Physics Expert group on divertor, database, and modelling, Nucl. Fusion 39 (1999) 2391.
[2] Federici, G., Skinner, C.H., Brooks, J.N., et al., Nucl. Fusion 41 (2001) 1967.
[3] Loarte, A., Lipschultz, B., Kukushkin, A.S., et al., Nucl. Fusion 47 (2007) S203.
[4] LaBombard, B., Hughes, J.W., Mossessian, D., et al., Nucl. Fusion 45 (2005) 1658.
[5] Scott, B., Plasma Phys. Contr. Fusion 39 (1997) 1635.
[6] Rogers, B.N., Drake, J.F., and Zeiler, A., Phys. Rev. Letters 81 (1998) 4396.
[7] Kallenbach, A., Dux, R., Gafert, J., et al., Nucl. Fusion 43 (2003) 573.
[8] Kallenbach, A., Asakura, N., Kirk, A., et al., J. Nucl. Mater. 337-339 (2005) 381.
[9] Harrison, M.F.A., Nucl. Technol./Fusion 3 (1983) 432.
[10] Lackner, K., Comments Plasma Phys. Controlled Fusion 15 (1994) 359.
[11] Jardin, S.C., Bathke, C.G., Ehst, D.A., et al., Fusion Eng. Design 48 (2000) 281.
[12] Loarte, A., Bosch, S., Chankin, A., et al., J. Nucl. Mater. 266-269 (1999) 587.
[13] Fundamenski, W., Pitts, R.A., Matthews, G.F., et al., Nucl. Fusion 45 (2005) 950.
[14] Kukushkin, A., Pacher, H.D., Coster, D., et al., Contr. Plasma Phys. 38 (1998) 20.
[15] Rudakov, D.L., Boedo, J.A., Moyer, R.A., et al., Nucl. Fusion 45 (2005) 1589.
[16] Whyte, D.G., Lipschultz, B., Stangeby, P.C., et al., Plasma Phy. & Cont. Fusion 47 (2005) 1579.
[17] Garcia, O.E., Horacek, J., Pitts, R.A., et al., Plasma Phys. Contr. Fusion 48 (2006) L1.
[18] Lipschultz, B., Whyte, D., and LaBombard, B., Plasma Phy. & Cont. Fusion 47 (2005) 1559.
[19] Leonard, A.W., Boedo, J.A., Groth, M., et al., J. Nucl. Mater. 363-365 (2007) 1067.
[20] Lipschultz, B., Andrew, P., Coad, J., et al., "A study of JET radial transport based on particle balance", (Proc. of the 30th European Conf. On Controlled Fusion and Plasma Physics, St. Petersburg, Russia, 2003), European Physical Society, Geneva.
[21] Kukushkin, A.S., Pacher, H.D., Pacher, G.W., et al., Nucl. Fusion 43 (2003) 716.
[22] Labombard, B., Lipschultz, B., Goetz, J., et al., "Cross-field transport in the SOL: Its relationship to main chamber and divertor neutral control in Alcator C-Mod" in Fusion Energy 2000 (Proc. 18th Int. Conf. Sorrento, 2000) (Vienna: IAEA) CD-ROM file [EX5/6] and http://www.iaea.org/programmes/ripc/physics/fec2000/html/node1.htm.
[23] Matthews, G.F., J. Nucl. Mater. 337-339 (2005) 1.
[24] Whyte, D.G., Coad, J.P., Franzen, P., et al., Nucl. Fusion 39 (1999) 1025.
[25] Lipschultz, B., Pappas, D.A., LaBombard, B., et al., J. Nucl. Mater. 290-293 (2001) 286.
[26] Baldwin, M.J., Schmid, K., Doerner, R.P., et al., J. Nucl. Mater. 337-339 (2005) 590.
[27] Greenwald, M., Terry, J.L., Wolfe, S.M., et al., Nucl. Fusion 28 (1988) 2199.
[28] LaBombard, B., Umansky, M.V., Boivin, R.L., et al., Nucl. Fusion 40 (2000) 2041.
[29] Antar, G.Y., Counsell, G., Yu, Y., et al., Phys. Plasmas 10 (2003) 419.
[30] Boedo, J.A., Rudakov, D.L., Moyer, R.A., et al., Phys. Plasmas 10 (2003) 1670.
[31] Terry, J.L., Zweben, S.J., Hallatschek, K., et al., Phys. Plasmas 10 (2003) 1739.
[32] Kirnev, G.S., Budaev, V.P., Grashin, S.A., et al., Nucl. Fusion 45 (2005) 459.
[33] Carter, T.A., Phys. Plasmas 13 (2006) 010701.

[34] Counsell, G.F., Ayed, B., Dendy, R., et al., "Analysis of L-mode turbulence in the MAST boundary plasma" in Fusion Energy 2006 (Proc. 21st Int. Conf. Chengdu, 2006) (Vienna: IAEA) CD-ROM file [EX/P4_6] and http://www-naweb.iaea.org/napc/physics/FEC/FEC2006/html/index.htm.
[35] Grulke, O., Terry, J.L., LaBombard, B., et al., Phys. Plasmas 13 (2006) 012306.
[36] Zweben, S.J., Maqueda, R.J., Terry, J.L., et al., Phys. Plasmas 13 (2006) 056114.
[37] Goncalves, B., Hidalgo, C., Silva, C., et al., J. Nucl. Mater. 337-339 (2005) 376.
[38] Myra, J.R., D'Ippolito, D.A., Stotler, D.P., et al., Phys. Plasmas 13 (2006) 092509.
[39] Carreras, B.A., J. Nucl. Mater. 337-339 (2005) 315.
[40] Zweben, S., Boedo, J., Grulke, O., et al., IEA Large Tokamak IA Workshop on Edge Transport in Fusion Plasmas, Krakow, Poland, 2006, "Edge Turbulence Measurements in Toroidal Fusion Devices", submitted to Plasma Physics and Controlled Fusion
[41] Naulin, V., J. Nucl. Mater. 363-365 (2007) 24.
[42] Conway, G.D., Kurzan, B., Scott, B., et al., Plasma Phys. Contr. Fusion 44 (2002) 451.
[43] Pitts, R., Horacek, W., Fundamenski, W., et al., J. Nucl. Mater. 363-365 (2007) 505.
[44] Naulin, V., "Turbulence Modeling of JET SOL Plasma" in Fusion Energy 2006 (Proc. 21st Int. Conf. Chengdu, 2006) (Vienna: IAEA) CD-ROM file [TH/P6_22] and http://www-naweb.iaea.org/napc/physics/FEC/FEC2006/html/index.htm.
[45] Pigarov, A.Y., Krasheninnikov, S.I., Rognlien, T.D., et al., Phys. Plasmas 9 (2002) 1287.
[46] Rognlien, T.D., Bulmer, R.H., Rensink, M.E., et al., J. Nucl. Mater. 363-365 (2007) 658.
[47] Pitts, R.A., Coad, J.P., Coster, D.P., et al., Plasma Phys. Contr. Fusion 47 (2005) B303.
[48] LaBombard, B., Rice, J.E., Hubbard, A.E., et al., Phys. Plasmas 12 (2005) 056111.
[49] Gunn, J.P., Boucher, C., Dionne, M., et al., J. Nucl. Mater. 363-365 (2007) 484.
[50] Erents, S.K., Pitts, R.A., Fundamenski, W., et al., Plasma Phys. Contr. Fusion 46 (2004) 1757.
[51] Pitts, R.A., Andrew, P., Arnoux, G., et al., "ELM Transport in the JET Scrape-Off Layer" in Fusion Energy 2006 (Proc. 21st Int. Conf. Chengdu, 2006) (Vienna: IAEA) CD-ROM file [EX/3_1] and http://www-naweb.iaea.org/napc/physics/FEC/FEC2006/html/index.htm.
[52] Hidalgo, C., Goncalves, B., Silva, C., et al., Phys. Rev. Letters 91 (2003) 65001/1.
[53] Eich, T., Herrmann, A., Neuhauser, J., et al., Plasma Phys. Contr. Fusion 47 (2005) 815.
[54] Fenstermacher, M.E., Osborne, T.H., Leonard, A.W., et al., Nucl. Fusion 45 (2005) 1493.
[55] Maingi, R., Bell, M.G., Fredrickson, E.D., et al., Phys. Plasmas 13 (2006) 092510.
[56] Kirk, A., Eich, T., Herrmann, A., et al., Plasma Phy. & Cont. Fusion 47 (2005) 995.
[57] Kirk, A., Ben Ayed, N., Counsell, G.F., et al., Plasma Phys. & Control. Fusion 48 (2006) B433.
[58] Fundamenski, W. and Sailer, W., Plasma Phys. Contr. Fusion 46 (2004) 233.
[59] Boedo, J.A., Rudakov, D.L., Hollmann, E., et al., Phys. Plasmas 12 (2005) 072516.
[60] Asakura, N., Ohno, N., Kawashima, H., et al., "ELM Propagation and Fluctuations Characteristics in H- and L-mode SOL Plasmas on JT-60U" in

Fusion Energy 2006 (Proc. 21st Int. Conf. Chengdu, 2006) (Vienna: IAEA) CD-ROM file [EX/D9_2] and http://www-naweb.iaea.org/napc/physics/FEC/FEC2006/html/index.htm.
[61] Maqueda, R., Maingi, R., Tritz, K., et al., J. Nucl. Mater. 363-365 (2007) 1001.
[62] Terry, J.L., Cziegler, I., Hubbard, A.E., et al., J. Nucl. Mater. 363-365 (2007) 995.
[63] Zeng, L., Wang, G., Doyle, E.J., et al., Plasma Phys. Contr. Fusion 46 (2004) A121.
[64] Kirk, A., Wilson, H.R., Akers, R., et al., Plasma Phys. Contr. Fusion 47 (2005) 315.
[65] Eich, T., Andrew, P., Fundamenski, W., et al., J. Nucl. Mater. 363-365 (2007) 990.
[66] Oyama, N., Sakamoto, Y., Isayama, A., et al., Nucl. Fusion 45 (2005) 871.
[67] Fundamenski, W., Pitts, R.A., and contributors, J.E., Plasma Phys. Contr. Fusion 48 (2006) 109.
[68] Loarte, A., Saibene, G., Sartori, R., et al., "ELMs and disruptions in ITER : Expected Energy Fluxes on Plasma-Facing Components from Multi-machine Experimental Extrapolations and Consequences for ITER Operation" in Fusion Energy 2006 (Proc. 21st Int. Conf. Chengdu, 2006) (Vienna: IAEA) CD-ROM file [IT/P1_14] and http://www-naweb.iaea.org/napc/physics/FEC/FEC2006/html/index.htm.
[69] Loarte, A., Saibene, G., Sartori, R., et al., Phys. Scr. T128 (2007) 222.
[70] Leonard, A.W., Groebner, R.J., Mahdavi, M.A., et al., Plasma Phys. Contr. Fusion 44 (2002) 945.
[71] Eich, T., Herrmann, A., Neuhauser, J., et al., Phys. Rev. Letters 91 (2003) 195003.
[72] Pitts, R.A., Andrew, P., Bonnin, X., et al., J. Nucl. Mater. 337-339 (2005) 146.
[73] Herrmann, A., Eich, T., Rohde, V., et al., Plasma Phys. Contr. Fusion 46 (2004) 971.
[74] Pitts, R.A., Fundamenski, W., Erents, S.K., et al., Nucl. Fusion 46 (2006) 82.
[75] McCracken, G.M., Lipschultz, B., Labombard, B., et al., Phys. Plasmas 4 (1997) 1681.
[76] Federici, G., Loarte, A., and Strohmayer, G., Plasma Phys. Contr. Fusion 45 (2003) 1523.
[77] Linke, J., "Material Damage Characterisation of Divertor Targets Exposed to ITER-Relevant Type I
ELM and Disruption Transient Loads" in Fusion Energy 2006 (Proc. 21st Int. Conf. Chengdu, 2006) (Vienna: IAEA) CD-ROM file [EX/4_5Rb] and http://www-naweb.iaea.org/napc/physics/FEC/FEC2006/html/index.htm.
[78] Zhitlukhin, A., Klimov, N.S., Landman, I., et al., J. Nucl. Mater. 363-365 (2007) 301.
[79] Khimchenko, L.N., Gureev, V.M., Federici, G., et al., "Study of erosion products in experiments simulating ELMs
and disruptions in ITER on plasma gun QSPA-facility" in Fusion Energy 2006 (Proc. 21st Int. Conf. Chengdu, 2006) (Vienna: IAEA) CD-ROM file [EX/4_5Ra] and http://www-naweb.iaea.org/napc/physics/FEC/FEC2006/html/index.htm.
[80] Loarte, A., Saibene, G., Sartori, R., et al., Phys. Plasmas 11 (2004) 2668.
[81] Lang, P.T., Conway, G.D., Eich, T., et al., Nucl. Fusion 44 (2004) 665.
[82] Evans, T.E., Moyer, R.A., Watkins, J.G., et al., J. Nucl. Mater. 337-339 (2005) 691.
[83] Loarte, A., "Expected energy fluxes onto ITER Plasma Facing Components during disruption thermal quenches from multi-machine data comparisons" in Fusion Energy 2004 (Proc. 20th Int. Conf. Villamoura, 2004) (Vienna: IAEA)

CD-ROM file [IT/P3_34] and http://www-naweb.iaea.org/napc/physics/FEC/FEC2004/datasets/index.html.
[84] Pautasso, G., Eich, T., Herrmann, A., et al., "Details of power deposition in the thermal quench of ASDEX-Upgrade disruptions", (Proc. of the 31st EPS Conference on Plasma Physics, London, U.K., 2004), P:4.132.
[85] Whyte, D.G., Jernigan, T.C., Humphreys, D.A., et al., J. Nucl. Mater. 313-316 (2003) 1239.
[86] Hollmann, E., "Disruption Thermal Quench Mitigation by Noble Gas Jet Injection in DIII-D" in Fusion Energy 2004 (Proc. 20th Int. Conf. Villamoura, 2004) (Vienna: IAEA) CD-ROM file [EX/10_6Ra] and http://www-naweb.iaea.org/napc/physics/FEC/FEC2004/datasets/index.html.
[87] Granetz, R., Whyte, D.G., Izzo, V.A., et al., Nucl. Fusion 46 (2006) 1001.
[88] Izzo, V.A., Nucl. Fusion 46 (2006) 541.
[89] Whyte, D.G. and Davis, J.W., J. Nucl. Mater. 337-339 (2005) 560.
[90] Whyte, D.G., West, W.P., Wong, C.P.C., et al., Nucl. Fusion 41 (2001) 1243.
[91] Philipps, V., "Overview of recent work on material erosion, migration and long-term fuel retention in the EU-fusion programme and conclusions for ITER " in Fusion Energy 2004 (Proc. 20th Int. Conf. Villamoura, 2004) (Vienna: IAEA) CD-ROM file [EX/10_1] and http://www-naweb.iaea.org/napc/physics/FEC/FEC2004/datasets/index.html.
[92] Loarer, T., Brosset, C., Bucalossi, J., et al., "Gas balance and fuel retention in fusion devices" in Fusion Energy 2006 (Proc. 21st Int. Conf. Chengdu, 2006) (Vienna: IAEA) CD-ROM file [Paper EX/3_6] and http://www-naweb.iaea.org/napc/physics/FEC/FEC2006/html/index.htm.
[93] Whyte, D., Lipschultz, B., Irby, J., et al., "Hydrogenic Fuel Recovery and Retention with Metallic Plasma-Facing Walls in the Alcator C-Mod Tokamak" in Fusion Energy 2006 (Proc. 21st Int. Conf. Chengdu, 2006) (Vienna: IAEA) CD-ROM file [EX/P4_29] and http://www-naweb.iaea.org/napc/physics/FEC/FEC2006/html/index.htm.
[94] Roth, J., Kirschner, A., Bohmeyer, W., et al., J. Nucl. Mater. 337-339 (2005) 970.
[95] Kirschner, A., Borodin, D., Droste, S., et al., J. Nucl. Mater. 363-365 (2007) 91.
[96] Wright, G., Whyte, D., Harrison, S., et al., J. Nucl. Mater. 363-365 (2007) 978.
[97] Walsh, D.S., Doyle, B.L., and Jackson, G.L., J. Vac. Sci. Technol. A 10 (1992) 1174.
[98] Skinner, C.H., Blanchard, W., Kamperschroer, J., et al., J. Vac. Sci. & Tech., A 14 (1996) 3267.
[99] Krieger, K., Jacob, W., Rudakov, D.L., et al., J. Nucl. Mater. 363-365 (2007) 871.
[100] Litnovsky, A., Philipps, V., Kirschner, A., et al., "Carbon transport, deposition and fuel accumulation in castellated structures exposed in TEXTOR", (Proc. of the 12th Int. Conf. on Fus. React. Mat., Santa Barbara, California, USA, 2005), 31842.
[101] Tanabe, T., Sugiyama, K., Skinner, C.H., et al., Fusion Sci. & Tech. 48 (2005) 577.
[102] Hsu, W.L., Mills, B.E., Ehrhardt, A.B., et al., J. Vac. Sci. & Tech., A 7 (1989) 1065.
[103] Kirschner, A., Philipps, V., Balden, M., et al., "Material Erosion and Redeposition during the JET MkIIGB-SRP Divertor Campaign" in Fusion Energy 2006 (Proc. 21st Int. Conf. Chengdu, 2006) (Vienna: IAEA) CD-ROM

file [EX/3_5] and http://www-naweb.iaea.org/napc/physics/FEC/FEC2006/html/index.htm.
[104] Litnovsky, A., Philipps, V., Wienhold, P., et al., Phys. Scr. T128 (2007) 45.
[105] Mayer, M., Rohde, V., and ASDEX Upgrade Team, Nucl. Fusion 46 (2006) 914.
[106] Pospieszczyk, A., Philipps, V., Casarotto, E., et al., J. Nucl. Mater. 241-243 (1997) 833.
[107] Tsitrone, E., J. Nucl. Mater. 363-365 (2007) 12.
[108] Loarer, T., Tsitrone, E., Brosset, C., et al., "Particle retention during long discharges in Tore Supra and JET", (Proc. of the 30th EPA Conference on Contr. Fusion & Plasma Phys., St Petersburg, Russia, 2003).
[109] Tsitrone, E., Brosset, C., Bucalossi, J., et al., "Deuterium retention in Tore Supra long discharges" in Fusion Energy 2004 (Proc. 20th Int. Conf. Villamoura, 2004) (Vienna: IAEA) CD-ROM file [EX/10_2] and http://www-naweb.iaea.org/napc/physics/FEC/FEC2004/datasets/index.html.
[110] Nakano, T., Asakura, N., Takenaga, H., et al., J. Nucl. Mater. 363-365 (2007) 1316.
[111] Loarer, T., Brygo, F., Gauthier, E., et al., J. Nucl. Mater. 363-365 (2007) 1451.
[112] Kubo, H., Nakano, T., Asakura, N., et al., "Particle Control under Wall Saturation in Long-pulse High-density H-mode Plasmas of JT-60U" in Fusion Energy 2006 (Proc. 21st Int. Conf. Chengdu, 2006) (Vienna: IAEA) CD-ROM file [EX/P4_11] and http://www-naweb.iaea.org/napc/physics/FEC/FEC2006/html/index.htm.
[113] Lipschultz, B., Lin, Y., Reinke, M.L., et al., Phys. Plasmas 13 (2006) 056117.
[114] Lipschultz, B., Lin, Y., Marmar, E.S., et al., J. Nucl. Mater. 363-365 (2007) 1111.
[115] Roth, J., Alimov, V.K., Golubeva, A.V., et al., J. Nucl. Mater. 363-365 (2007) 823.
[116] Alimov, V.K. and Roth, J., Phys. Scr. T128 (2007) 6.
[117] Skinner, C.H., Coad, J.P., and Federici, G., Phys. Scr. T111 (2004) 92.
[118] Counsell, G.F., Coad, J.P., Grisolia, C., et al., Plasma Phys. & Contr. Fusion 48 (2006) B189.
[119] Hu, J., Li, J.G., Wang, X.M., et al., J. Nucl. Mater. 363-365 (2007) 863.
[120] Doerner, R.P., Baldwin, M.J., Krasheninnikov, S.I., et al., J. Nucl. Mater. 337-339 (2005) 877.
[121] Wiltner, A. and Linsmeier, C., New Journal of Physics 8 (2006) 181.
[122] Linsmeier, C., Ertl, K., Roth, J., et al., J. Nucl. Mater. 363-365 (2007) 1130.
[123] Roth, J., Wampler, W.R., and Jacob, W., J. Nucl. Mater. 250 (1997) 23.
[124] Ogorodnikova, O.V., Roth, J., and Mayer, M., J. Nucl. Mater. 313-316 (2003) 469.
[125] Schmid, K., Baldwin, M., and Doerner, R., J. Appl. Phys. 97 (2005) 064912.
[126] Roth, J., J. Nucl. Mater. 266-269 (1999) 51.
[127] Balden, M., Adelhelm, C., de Juan Pardo, E., et al., J. Nucl. Mater. 363-365 (2007) 1174.
[128] Chen, J.L. and Li, J.G., J. Nucl. Mater. 363-365 (2007) 1335.
[129] Philipps, V., Pospieszczyk, A., Unterberg, B., et al., J. Nucl. Mater. 212-215 (1994) 1189.
[130] Bolt, H., Barabash, V., Federici, G., et al., J. Nucl. Mater. 307-311 (2002) 43.
[131] Barabash, V., Federici, G., Linke, J., et al., J. Nucl. Mater. 313-316 (2003) 42.
[132] Gasparotto, M., Andreani, R., Boccaccini, L.V., et al., Fusion Eng. Design 66-68 (2003) 129.
[133] Causey, R., Wilson, K., Venhaus, T., et al., J. Nucl. Mater. 266-269 (1999) 467.

[134] Neu, R., Bobkov, V., Dux, R., et al., J. Nucl. Mater. 363-365 (2007) 52.
[135] Wukitch, S., Lipschultz, B., Marmar, E.S., et al., J. Nucl. Mater. 363-365 (2007) 491.
[136] Dux, R., Bobkov, V., Fedorczak, N., et al., J. Nucl. Mater. 363-365 (2007) 112.
[137] Matthews, G.F., Edwards, P., Hirai, T., et al., Phys. Scr. T128 (2007) 137.
[138] Lisgo, S., Borner, P., Boswell, C., et al., J. Nucl. Mater. 337-339 (2005) 139.
[139] Kukushkin, A.S., Pacher, H.D., Kotov, V., et al., Nucl. Fusion 45 (2005) 608.
[140] Kotov, V., Reiter, D., Kukushkin, A., et al., Contr. Plasma Phys. 46 (2006) 635.
[141] Kukushkin, A.S., Pacher, H.D., Kotov, V., et al., "Effect of Pumped Gas Reflux on Divertor Operation in ITER" in Fusion Energy 2006 (Proc. 21st Int. Conf. Chengdu, 2006) (Vienna: IAEA) CD-ROM file [IT/P1_16] and http://www-naweb.iaea.org/napc/physics/FEC/FEC2006/html/index.htm.
[142] Riemann, J., Borchardt, M., Schneider, R., et al., J. Nucl. Mater. 313-316 (2003) 1030.
[143] Urano, H., Suttrop, W., Lang, P.T., et al., Plasma Phys. Contr. Fusion 46 (2004) A315.